Geosci. Model Dev. Discuss., https://doi.org/10.5194/gmd-2017-207
Manuscript under review for journal Geosci. Model Dev.
Discussion started: 6 November 2017

Geoscientific Model Development Discussions

Evaluating a fire smoke simulation algorithm in the National Air Quality Forecast Capability (NAQFC) by using multiple observation data sets during the Southeast Nexus (SENEX) field campaign

Li Pan [1,2], Hyun Cheol Kim [1,2], Pius Lee [1], Rick Saylor [3], YouHua Tang[1,2], Daniel Tong [1,2], Barry Baker[1,2], Shobha Kondragunta [4], Chuanyu Xu [5], Mark G. Ruminski [4], Weiwei Chen [1,6], Jeff Mcqueen [7] and Ivanka Stajner[8]

[1] NOAA/OAR/Air Resources Laboratory, College Park, MD 20740, USA

[2] UMD/Cooperative Institute for Climate and Satellites, College Park, MD 20740, USA

[3] NOAA/OAR/ARL/Atmospheric Turbulence and Diffusion Division, Oak Ridge, TN 37830, USA

[4] NOAA/NESDIS, College Park, MD 20740, USA

[5] I. M. Systems Group at NOAA, College Park, MD 20740, USA

[6] Northeast Institutes of Geography and Agroecology, Chinese Academy of Sciences, Changchun 130102, P. R. China

[7] NOAA/NCEP/Environmental Modeling Center, College Park, MD 20740, USA

[8] NOAA/NWS Office of Science and Technology Integration, Silver Spring, MD 20910, USA

Correspondence to: Li.Pan@noaa.gov

Geosci. Model Dev. Discuss., https://doi.org/10.5194/gmd-2017-207
Manuscript under review for journal Geosci. Model Dev.
Discussion started: 6 November 2017

Geoscientific Model Development Discussions
Open Access

Abstract

Multiple observation data sets, including Interagency Monitoring of Protected Visual Environments (IMPROVE) network data, Automated Smoke Detection and Tracking Algorithm (ASDTA), Hazard Mapping System (HMS) smoke plume shapefiles and aircraft acetonitrile (CH_3CN) measurements from the NOAA Southeast Nexus (SENEX) field campaign are used to evaluate the HMS-BlueSky-SMOKE-CMAQ fire emissions and smoke plume prediction system. A similar configuration is used in the National Air Quality Forecasting Capability (NAQFC). The system was found to capture signatures of most of the observed fire signals. Use of HMS-detected fire hotspots and smoke plume information are valuable for both initiating fire emissions and evaluating model simulations. However, we also found that the current system does not include fire contributions through lateral boundary condition and missed fires that are not associated with visible smoke plumes resulting in significant simulation uncertainties. In this study we focused not only on model evaluation but also on evaluation methods. We discuss how to use observational data correctly to filter out fire signals and synergistic use of multiple data sets together. We also address the limitations of each of the observation data sets and of the evaluation methods.

Introduction

Wildfires and agricultural prescribed burns are common in North America all year round, but predominantly occur during the spring and summer months (Wiedinmyer et al., 2006). These fires pose a significant risk to air quality and human health (Delfino et al., 2009; Rappold et al., 2011; Dreessen et al., 2016; Wotawa and Trainer 2000; Sapkota et al., 2005; Jaffe et al., 2013; Johnston et al., 2012). Therefore, since January 2015, smoke emissions from fires have been included in the National Air Quality Forecasting Capability (NAQFC) daily $PM_{2.5}$ operational forecast (Lee et al., 2017). The NAQFC fire simulation consists of the NOAA National Environmental and Satellite Data and Information Service (NEDIS) Hazard Mapping System (HMS) fire detection algorithm, the U.S. Forest Service (USFS) BlueSky-fire emissions estimation algorithm, the U.S. EPA Sparse Matrix operator Kernel Emission (SMOKE) applied for fire plume rise calculations, the NOAA National Weather Service (NWS) North American Multi-scale Model (NAM) for meteorological prediction and the U.S. EPA Community Multi-scale Air Quality Model (CMAQ) for chemical transport and transformation. In contrast to most anthropogenic emissions, smoke emissions from fires are largely uncontrolled, transient and unpredictable. As a result, quantitative description of fire emissions and their impact on air pollution remains a substantial challenge for air quality forecasting (Pavlovic et al., 2016; Lee et al., 2017; Huang et al., 2016).

Southeast Nexus (SENEX) was a NOAA field study conducted in the Southeast U.S. in June and July 2013 (Warneke et al., 2016). This field experiment investigated the interactions between natural and anthropogenic emissions and their impact on air quality and climate change (Xu et al., 2016; Neuman et al., 2016). In this work, we use the rich SENEX dataset to evaluate HMS-BlueSky-SMOKE-CMAQ fire simulations during the campaign period.

Two simulations were performed in this study, one with and one without smoke emissions from fires during the SENEX field campaign. Due to the large uncertainties of fire emissions and smoke simulations (Baker et al., 2016; Davis et al., 2015; Drury et al., 2014), the first step of the evaluation focused on the fire signal capturing capacity of the system. Differences between the two simulations represent the impact of the smoke emissions from fires on the CMAQ model results. Observations from various sources were utilized in this analysis: (i) ground observations (Interagency Monitoring of Protected Visual Environments (IMPROVE)), (ii) satellite retrievals (Automated Smoke Detection and Tracking Algorithm (ASDTA) and HMS smoke plume shape), and (iii) aircraft measurements (SENEX campaign). Fire signals predicted by the modeling system are directly compared to these observations, and several criteria are used to rank sensitivities of the observations to fires.

Methodology

In this section we introduce the NAQFC fire modeling system used in the study. Uncertainties and limitations in the various modeling components of the system are discussed. Fig. 1 illustrates the schematics of the system. There are four processing steps:

HMS (Hazard Mapping System)

The NOAA NEDIS HMS is a fire smoke detection system based on satellite retrievals. The satellite constellation used comprises of 2 Geostationary Operational Environmental Satellite (GOES-10 and GOES-12) and 5 polar orbiting satellites (MODIS (Moderate-resolution Imaging Spectroradiometer)) -- Terra and Aqua, AVHRR (Advanced Very High Resolution Radiometer) 15/17/18). HMS detects fire (wildfires and agricultural/prescribed) locations and analyses their sizes, starting times and durations (Ruminski et al., 2008; Schroeder et al., 2008; Ruminski and Kondragunta 2006).

HMS first processes satellite data to detect fire locations utilizing automated algorithms for each of satellite platforms (Justice et al., 2002; Giglio et al., 2003; Prins and Menzel 1992; Li et al., 2000) and subsequently conducts data analyst process manually by human analysts to eliminate false detections and/or add missed fire hotspots for data quality control purpose as well as to estimate fire sizes, starting times and durations from close inspection of visible band satellite imagery. The sizes of fire are represented in the form of numbers of detecting pixels whose size is corresponded to the nominal resolution of MODIS or AVHRR data. A bookkeeping file is generated at the end of this detection step, named “hms.txt”, and includes all the thermal signal hotspots detected by the aforementioned 7 satellites. During the analyst quality control step, detected potential fire hotspots lacking visible smoke in the retrieval's RGB real-color imagery are removed resulting in a reduced fire hotspot file called either "hmshysplit.prelim.txt" or "hmshysplit.txt" to be input into the BlueSky processing step.

In general, "hmshysplit.prelim.txt" and "hmshysplit.txt" are very similar, and "hmshysplit.txt" is created later than "hmshysplit.prelim.txt" (Fig. 1). But the differences between "hmx.txt" and "hmshysplit.txt" ("hmshysplit.prelim.txt") can be rather substantial. The reasons for differences are: 1) many detected fires do not produce detectable smoke; 2) some fires/hotspots are detected only at night, when smoke detection is not possible; 3) smoke emissions are obscured by clouds or not detected by the analyst. Therefore, smoke emission occurrence provided by the HMS is a conservative estimate of overall emissions.

Using multiple satellites, the likehood of detecting fires in HMS has been improved. However, when the fire geographical size is small, the HMS detection rate and accuracy dramatically decreases (Zhang et al., 2011; Hu et al., 2016). Other limitations of the HMS fire detections include ineffective retrievals at nighttime and under cloud cover.

BlueSky

BlueSky, developed by the USFS (US Forest Service), is a modelling framework to simulate smoke impacts on regional air quality (Larkin et al., 2009; Strand et al., 2012). In this study, BlueSky acts as a fire emission model to provide input for SMOKE (Herron-Thorpe et al., 2014; Baker et al., 2016). BlueSky calculates fire emission locations in the map projection of the meteorological model and uses fire geographical extent based on HMS-derived parameters (Fig. 1).

Fire extent is reflected by the number of nearby fire pixels detected in a 12 km resolution model grid by satellites. Fire pixels are converted to fire burning areas used in BlueSky based on the assumption that each fire pixel has a size of 1 km^2 and 10% of its area can be considered as active (Rolph

Geosci. Model Dev. Discuss., https://doi.org/10.5194/gmd-2017-207
Manuscript under review for journal Geosci. Model Dev.
Discussion started: 6 November 2017

et al., 2009). All fire pixels in a 12 km grid square are aggregated. To estimate how much biomass is available, fuel loading map used in BlueSky is from US National Fire Danger Rating System (NFDRS) for CONUS, except in western US it is from HARDY (Hardy and Hardy 2007). And, BlueSky uses Emissions Production Model (EPM) (Sandberg and Peterson 1984), a simple version of CONSUME, to calculate how much of it will actually be burned -- the so-called consumption sums. Finally, EPM is also used in BlueSky to calculate the fire emission rate i.e., how fast the fuel will be burned hourly over each fire grid-cell. BlueSky outputs CO, CO_2, CH_4, non-methane hydrocarbons (NMHC), total PM, $PM_{2.5}$, PM_{10} and heat flux (Fig. 1).

BlueSky does not recalculate fire duration according to the fuel loading map or the modeled fire burning behavior. Also, as part of the aggregation process, when there is more than one HMS point in a grid cell and they have different durations, the aggregation would assign the largest duration to all points in that grid cell. For example, if there were 3 HMS points that had durations of 10, 10 and 24 hours, the aggregation would include 3 points (representing 3 km^2) but would assign 24 hour duration to all of the points.

Since HMS has no information about fuel loading, BlueSky uses a default fuel loading climatological inventory database over eastern US. BlueSky uses an idealized diurnal temporal profile for fire emission. Obviously, uncertainties in fire sizes, fuel loading and fire emission rate will lead to large uncertainties in smoke emissions from fires (Knorr et al., 2012; Drury et al., 2014; Davis et al., 2015).

SMOKE

In SMOKE (Sparse Matrix Operator Kernel Emission), the BlueSky fire emissions data in a longitude/latitude map projection are converted to gridded CMAQ ready emission files (Fig. 1). Fire smoke plume rise is calculated using formulas by Briggs'; the heat flux from BlueSky and NAM meteorological state variables are used as input (Erbrink 1994). The Brigg's algorithm calculates plume

Geosci. Model Dev. Discuss., https://doi.org/10.5194/gmd-2017-207
Manuscript under review for journal Geosci. Model Dev.
Discussion started: 6 November 2017

Geoscientific Model Development Discussions
Open Access

top and plume bottom. Between plume top and bottom the emission fraction was calculated layer by layer assuming a linear distribution of flux strength in atmospheric pressure. For model layers below the plume bottom the emission fraction is assumed to be entirely in the smoldering condition as a function of the fire burning area.

Speciation cross-reference maps match BlueSky chemical species to CMAQ chemical species by using the U.S. EPA Source Classification Codes (SCCs) refers to emissions from forest Wildfires (https://ofmpub.epa.gov/sccsearch/docs/SCC-IntroToSCCs.pdf). The temporal distribution of fire is based on the HMS detected fire starting time and duration. During fire burning hours a constant emission rate is assumed. This constant burn-rate assumption has been shown to be a crude estimate (Saide et al., 2015; Alvarado et al., 2015). Other uncertainties include plume rise (Sofiev et al., 2012; Urbanski et al., 2014; Achtemeier et al., 2011) and fire-weather (fire influencing local weather).

CMAQ

CMAQ version 4.7.1 was used for the simulations in this study, using the CB05 gas phase chemical mechanism (Yarwood et al., 2005) and the AERO5 aerosol module (Carlton et al., 2010). Anthropogenic emissions were based on the U.S. EPA 2005 National Emission Inventory (NEI) projected to 2013 (Pan et al., 2014), Biogenic emissions (BEIS 3.14) were calculated in-line in CMAQ. The NOAA NCEP NAM provided meteorology fields to drive CMAQ similarly to that in the operational NOAA NAQFC (Chai et al., 2013). The simulation domain is shown in Fig. 1 and includes two domains: (i) a 12km horizontal resolution domain covering the Continental U.S. (CONUS); and (ii) a 4km horizontal resolution domain covering the Southeast U. S., where the majority of SENEX measurements occurred. Boundary conditions used in the smaller SENEX domain simulation were extracted from CONUS simulations. Four scenarios were simulated: CONUS with fire emission, CONUS without fire emission, SENEX with fire emission and SENEX without fire emission.

Geosci. Model Dev. Discuss., https://doi.org/10.5194/gmd-2017-207
Manuscript under review for journal Geosci. Model Dev.
Discussion started: 6 November 2017

Evaluations

Carbon monoxide (CO) has a relatively long life time in the air and is commonly associated with biomass burning. CO was used as a fire tracer in the prediction and CO difference (ΔCO) between CMAQ simulation with and without fire emissions was used as the indicator of fire influence. For additional observations, we used potassium (K) collected at the IMPROVE (Interagency Monitoring of Protected Visual Environments) sites within the SENEX domain, acetonitrile (CH_3CN) measured from the SENEX campaign flights and fire plume shape detected by the HMS analysis as real fire signals. Temporal enhancement (Δ) in CO concentration due to fire denoted as ΔCO was directly compared with those signals. At the same time, ΔAOD (Aerosol Optical Depth) from CMAQ ("withfire" simulated concentration minus that with "nofire") was also used as fire indicator when compared with smoke masks given by ASDTA (Automated Smoke Detection and Tracking Algorithm).

In this study, we have focused on qualitative evaluations subject to the large uncertainties of the underlying physical processes of smoke emissions from fires and its transport. In each modeling step in HMS, BlueSky, SMOKE and CMAQ, the modeling system accrues uncertainties, which are likely cumulative and might lead to larger error in succeeding components (Wiedinmyer et al., 2011). For example, heat flux from BlueSky influenced plume rising height in SMOKE and consequently influenced plume transport in CMAQ. It is also noteworthy that when we compared modeled ΔCO against measured K or CH_3CN, the objective was to scour for enhancement signals resulting from fires but it was not aiming to account for proportional concentration changes in the tracers. Attempting to account for CMAQ simulation biases in surface ozone and particulate matter as a function of smoke emissions from fires was difficult and not the objective of this study. Rather, the purpose of this study is to focus on analyzing the capability of the HMS-BlueSky-SMOKE-CMAQ modeling system to capture the timing of fire signals.

The SENEX campaign occurred in June and July and our model simulations were from June 10 to July 20, 2013. Throughout the campaign we used all available observation datasets including ground-, air- and satellite-based acquired data. Each dataset had its unique characteristics and linking them together gave an overall evaluation. At the same time, in each dataset our evaluations included as many as possible observed fire cases. Both well-predicted and poorly-predicted cases are presented to illustrate potential reasons responsible for the modeling system's behavior.

Results and Discussions

Observed CO versus modeled CO in SENEX

Tab. 1 lists observed and modeled CO vertical profiles for the "withfire" and "nofire" cases during the SENEX campaign. Observed CO concentration between the surface and 7 km attitude in the SENEX domain area remained greater than 100ppb during all 40 days of the campaign. The highest CO concentrations were measured closer to the surface. The maximum measured CO concentration of 1277 ppb was observed during a flight on July 03 at an altitude of 974 m. In this flight, strong fire signals were observed but the fire simulation system missed those signals, as discussed below.

CO concentrations were underestimated by the model in almost all cases even when the model captured CO contribution from fire emissions spatio-temporarily. Mean ΔCO in each height interval was usually above 1.5 ppb but less than 2.0 ppb. Fig. 2a exhibits the contribution of total CO emissions from fires which occurred inside the SENEX domain over the simulation period, the maximum CO emissions contribution from fires was about 3% during the campaign. In most of those days, fire emission contributions in SENEX were less than 1%. The averaged contribution during those 40 days was 0.7%. Fig. 2b exhibits the contribution of CO flux flowing into the SENEX domain from its boundary caused by fire burning outside the SENEX domain but inside the CONUS domain (Fig. 1). The averaged fire contribution to CO from outside the SENEX domain was 0.67%. CO influenced by fire emission in June is greater than that in July.

During the field experiment the general lack of large fires made evaluation of modeled fire signature difficult since it is easier to capture large fire signals than those from routine/small events. We postulated that a clear fire signal simulated in the HMS-BlueSky-SMOKE-CMAQ system can be represented by ΔCO significantly larger than its temporal averages considering both the fire originated from inside and outside the SENEX domain. For example, if a clear fire signal between 500 m and 1000 m altitude is represented by ΔCO in model simulation, the concentration of ΔCO is above 2.0 ppb, based on the average CO concentration of about 150 ppb as well as on with SENEX domain and outside of SENEX domain fire contributions of (150*(0.007+0.0067)=2.0).

Fig. 3 displays the simulated ΔCO extracted along a SENEX flight path. From the model perspective despite of lack of larger fire events as shown in Fig. 2a and 2b during SENEX campaign period, the fire impacts on SENEX were not negligible as shown on Fig. 3. That confirmed the importance of evaluating the fire simulation system in our air quality model. Unless a model is able to predict fire signals correctly, it is useless for modelers to discuss fire effects on chemical composition of the atmosphere. A detail of how our model caught or missed or falsely predicted fire signals during the SENEX campaign and a comparison of ΔCO versus CH_3CN will be discussed in the follow sections.

IMPROVE

The Interagency Monitoring of Protected Visual Environments (IMPROVE) is a long term air visibility monitoring program initiated in 1985 (http://vista.cira.colostate.edu/Improve/data-page). It provides 24 h integrated particulate matter (PM) speciation measurements every third day (Malm et al., 2004; Eatough et al., 1996). The IMPROVE dataset was chosen for this analysis because it includes K

Geosci. Model Dev. Discuss., https://doi.org/10.5194/gmd-2017-207
Manuscript under review for journal Geosci. Model Dev.
Discussion started: 6 November 2017

(potassium), OC (organic carbon) and EC (elemental carbon), important fire tracers, but also as ground observations the IMPROVE sites may likely be influenced by nearby fire sources.

There are 14 IMPROVE sites in the SENEX domain (Fig. 4). Potential fire signals were identified by using CMAQ modeled ΔCO and IMPROVE observed K. However, in addition to fires, K has multiple sources such as soil, sea salt and fertilizer industry. Since fires should also produce enhanced EC and OC concentrations, a fire signal should reflect corresponding above-average values for EC, OC, and K. EC, OC and K observations that were 20% above their temporal averages during the SENEX campaign were used as a filter for fire event identification. Meanwhile, co-measured NO_3^- and SO_4^{2-} concentrations 50% below their respective temporal averages was used to screen out data with industrial influences. Lastly, a third filter was employed so that concentrations of soil components should be below their temporal average to eliminate K sources from dust. With these three criteria the IMPROVE data was screened for fire events (shown in Tab. 2).

Five fire events were observed at four IMPROVE sites. Tab. 2 lists measured EC, OC, NO_3^-, K, soil and SO_4^{2-} concentrations (μg m^{-3}) and their ratios to averages. BC versus OC and K versus BC ratios were also calculated and listed in Tab. 2 to illustrate our criteria. We found that except for monitor BRIS, all other sites (COHU, MACA and GRSM) had BC/OC and K/BC ratios in the range of biomass burning reported by other researchers (Reid et al., 2005; DeBell et al., 2004). BRIS is a coastal site thus might have been influenced by sea salts (Fig. 4).

For the four identified fire cases, we plotted ΔCO as a modeled fire tracer around the IMPROVE sites. Our model simulation reproduced fire signals on June 21 at COHU and GRSM and on June 24 at MACA. We used the June 24 MACA case as an example (see Fig. 4) -- closed black circles represent the detected fire locations; open triangles represents IMPROVE sites, and only ΔCO values above 2.0 ppb are shown. On June 24, 2013, detected fire spots were outside the SENEX domain, but SSW wind blew

Geosci. Model Dev. Discuss., https://doi.org/10.5194/gmd-2017-207
Manuscript under review for journal Geosci. Model Dev.
Discussion started: 6 November 2017

smoke plumes into the SENEX domain and affected modeled CO in MACA. Modeled ΔCO in MACA was 5 ppb.

Another IMPROVE site located upwind of MACA, CADI, was also potentially under the influence of that fire event; however, data from CADI on June 24 did not indicate a fire influence, possibly due to the frequency of IMPROVE sampling that eluded measurement or that the smoke plume was transported further above the surface than it was modeled. Within the four fire cases identified by IMPROVE data during SENEX (Tab. 2), the model successfully captured three of them. The model missed fire signal on July 3 at MACA. The rationales the model missed the fire signal on July 3 at MACA was discussed in a section dedicated for the July 3 SENEX flight.

Plume Spatial Coverage

HMS determines fire hotspot locations associated with smoke and upon incorporating the smoke plume shape information from visible satellite images HMS provides smoke plume shapefiles over much of North America. We focused on the shapefile over CONUS – a two-dimensional smoke plume spatial depiction collapsing all plume stratifications to a satellite eye-view. For modeled plumes, we integrated modeled ΔCO by multiplying the layer values with the corresponding CMAQ model layer thicknesses and air density to derive a simulated smoke plume shape. HMS-derived smoke plume shape versus CMAQ predicted smoke plume shape was then used to evaluate the fire simulation.

Figure of Merits in Space (FMS) (Rolph et al., 2009) is a statistic for spatial analysis and was calculated as follows:

$$\mathrm{FMS} = \frac{\mathrm{Area\_hms} \ \cap \ \mathrm{Area\_cmaq}}{\mathrm{Area\_hms} \ \cup \ \mathrm{Area\_cmaq}} \ \mathrm{X}\ 100\%$$

Where Area_hms represents area of grid cells influenced by fire emission over CONUS detected by HMS and Area_cmaq represents area of grid cells over CONUS identified by model prediction. In general, a higher FMS value indicates a better agreement between the observed and modeled plume shape.

Fig. 5 summarizes FMS during the SENEX campaign. Average FMS was 22% with its maximum at 56% on July 6 and minimum at 1.2% on June 17. Fig. 6a exhibits HMS detected smoke plume and CMAQ calculated smoke plume over CONUS on July 6 2013. The light blue shading represents modeled plume shape (defined as total column ΔCO) and the thin dash line and emboldened green lines encircle areas representing HMS-derived light and strong influenced plume shape, respectively (Fig. 6a). The FMS score is 56% meaning that the modeled plume shape was consistent with that of HMS. However, CMAQ might have underestimated the intensive fire influence areas along the border of California and Nevada. Subsequently, the model also under-predicted its associated influence in North Dakota, South Dakota, Minnesota, Iowa and Wisconsin.

Fig. 6b exhibits the worst case on June 17, 2013, in our smoke plume shape prediction during SENEX where the FMS score was 1.2%. Two reasons led to this result: (i) CMAQ missed fire emissions from Canada since those fire sources are located outside the CONUS modeling domain and our simulation system used a climatologally-based static boundary condition. Secondly, on June 17 there were a lot of fire hotspots in the Southeastern U.S., i.e., in Louisiana, Arkansas and Mississippi along Mississippi River as detected by HMS but lacked detected associated smoke by HMS (Fig. 6c). This could be due to cloud blockage or to small agricultural debris clearing or prescribed burns. These conditions prevented HMS satellites from identifying fires and hence emissions were not modeled for those sources.

It is noteworthy that the FMS evaluation contained uncertainties contributed from both modeled and observed values. The calculated campaign duration and SENEX-wide averaged FMS was

22%. It is significantly higher than that achieved by a similar analyses done by HYSPLIT (Hybrid Single Particle Lagrangian Integrated Trajectory) smoke forecasting for the fire season of 2007 (6.1% to 11.6%) (Rolph et al., 2009). The primary reason is that the HYSPLIT smoke simulation accessed the HMS fire information at the invocation of a forecast cycle is already one day old due to satellite retrieval and HMS data latency issues. However, our model simulation in this study was from a retrospective module using current day HMS fire information. This led to results as shown here. Such discrepancies have been discussed by Huang et al. 2017 (*manuscript in preparation*). Other reasons, such as plume rising etc. were discussed in the section of ASDTA.

ASDTA

The Automated Smoke Detection and Tracking Algorithm (ASDTA) is a combination of two data sets: (1) the NOAA Geostationary satellite (G13) retrieves aerosol optical depth using visible channels and produces a product called GOES Aerosol/Smoke Product (GASP) (Prados et al., 2007); and, (2) the NOAA HYSPLIT dispersion model predicts smoke plume direction and extension (Draxier and Hess 1998). ASDTA provides the capability to determine whether the GASP is influenced by one or multiple smoke plumes over a location at a certain time. The ASDTA is a qualitative analysis. On the other hand, the HYSPLIT smoke forecast is based on the HMS fire detection and BlueSky emission modeling driven by the NOAA NWS meteorology model. These data formed a suitable basis to evaluate the model performance in this study. For each simulation, modeled AOD was calculated for each sensitivity test ("withfire" or "nofire") and ΔAOD is defined as the difference obtained by subtracting AOD_nofire from AOD_withfire.

Fig. 7a illustrates a GOES retrieved AOD (summed over from 10:00 am to 2:00 pm at local time) contour plot that reflects influences by smoke plumes over the CONUS domain on June 14, 2013. Color-shaded region represents the fire-smoke influenced areas and the color denotes the magnitude of the

Geosci. Model Dev. Discuss., https://doi.org/10.5194/gmd-2017-207
Manuscript under review for journal Geosci. Model Dev.
Discussion started: 6 November 2017

Geoscientific Model Development Discussions

retrieved AOD (Fig. 7a). Fig. 7b presents similar results, but for simulated ΔAOD (withfire – nofire). For further evaluation the HMS detected smoke plume shape (Fig. 7c) can be compared with Figs. 7a and 7b.

Fig. 7a shows several regions under the influence of fires: in California, northwest Mexico, Kansas, Missouri, Oklahoma, Arkansas, Texas and part of the Gulf of Mexico. In the northeastern U.S., fire plumes occurred sparingly. Those regions agreed relatively well with the shaded contours between Figs. 7a and 7c. However, due to the lack of fire treatments in the CMAQ lateral boundary conditions (LBC), the simulation (Fig. 7b) missed smoke influence on the northeast region of the CONUS domain. CMAQ also failed to regenerate the fire influences in the southwest region of the domain.

Similar plots for June 25 are shown in Figs. 7d, 7e and 7f for ASDTA, CMAQ and HMS, respectively. The ASDTA (Fig. 7d) predicted an overestimation in fire influences in the south including Texas and the Gulf of Mexico and an underestimation in the northeastern U.S. On the other hand, the model predicted two strong fire signals clearly: near the border between Arizona and Mexico, and in Colorado (See Fig. 7e). All the fire influenced areas in Fig. 7e were seen in Fig. 7f --- reflecting observation by HMS.

Comparing ASDTA plots and CMAQ ΔAOD plots (Fig. 7a vs 7b; Fig. 7d vs 7e), we found both similarities and differences. Similarities were attributable to similar fire accounting, smoke emissions from fires calculation and meteorology. Differences were attributable to: (i) HYSPLIT smoke simulation using more fire hotspots than that done by CMAQ due to domain size; only fires inside the CONUS have been included in the CMAQ fire simulation and LBCs did not vary to reproduce impacts of wildfires from outside of the domain. (ii) Despite both the HYSPLIT and CMAQ fire plume rises being estimated by the Brigg's equation, the HYSPLIT plume rise was limited to 75% of the mixed layer height (MLH) at daytime and 2×MLH at nighttime, whereas the CMAQ fire plume rise did not have these limitations.

SENEX

SENEX (Southeast Nexus) was a field campaign conducted by NOAA in cooperation with the U. S. EPA and the National Science Foundation in June and July 2013. Although SENEX was not specifically designed for fire studies, its airborne measurements included PM2.5 OC and EC, CO and acetonitrile (CH_3CN). CH_3CN was chosen as a fire tracer since it is predominantly emitted from biomass burning (Holzinger et al., 1999; Singh et al., 2012).

CH_3CN has a residence time in the atmosphere of around 6 months (Hamm and Warneck 1990) and the reported CH_3CN background concentration is around 100 - 200 ppt (Singh et al., 2003). Measured CH_3CN concentrations tend to increase with altitude (Singh et al., 2003; de Gouw et al., 2003), since biomass burning plumes are subject to ascend during long-range transport. During SENEX, measured CH_3CN showed a similar pattern. Fire signals were identified through airborne measurements of CH_3CN when its concentration exceeded the background; e.g., on July 3 2013, or when its concentration peak appeared at high altitude; e.g., on June 16 2013 and July 10 2013.

CH_3CN airborne measurements were used to identify fire plumes at certain locations and heights during SENEX. For model evaluations, fire locations and an accurate meteorological wind field are crucial to characterize 2-D measurements such as IMPROVE, HMS and ASDTA. To verify a 3-D fire field, it is critical to capture plume rise; however, it was extremely difficult to back out plume rise from the airborne measurements. An additional uncertainty arises in differing temporal resolutions of the data: IMPROVE, HMS shapefiles and ASDTA were daily or hourly data, whereas airborne CH_3CN data were measured at one-minute intervals.

Fig. 8a shows a CMAQ simulated ΔCO vertical distribution along flight transects on June 16 2013. This flight occurred during the weekend over and around power plants around Atlanta, GA. The color of flight path represents observed CH_3CN concentration (ppt). In Fig. 8a, the concentration of ΔCO increased from surface to 5000 m, especially above 2000 m. Six CH_3CN concentration peaks were observed when altitude was above 2500m.

For CMAQ simulated ΔCO, five out of six fire signals detected by CH_3CN measured spikes were captured where ΔCO concentrations were all above 3 ppb. Only one fire signal was missed by the model at 18:30 UTC June 16 2013. Model simulation showed that long range transports (LRT) of smoke plumes influenced airborne observations. Fire signals from the free troposphere subsided and influenced flight measurements. High EC or OC or CO did not concur with high CH_3CN observation probably due to species lifetime differences. HMS smoke plume did not show any hotspots or smoke plume around Atlanta suggesting that the sources of those observed fire signals were not from its vicinity.

A similar phenomenon was seen in SENEX flight 0710, which occurred during flight transects from Tennessee to Tampa, FL. Fig. 8b is a similar graph as Fig. 8a. Based on ΔCO concentrations CMAQ captured the July 10 case as fire signals were observed. Nonetheless, ΔCO may be over predicted at around 19 UTC. The model exhibited a fire signal with ΔCO concentration of about 3 ppb near 6000 m around 19 UTC, whereas measured CH_3CN was 120 ppt and decreased with altitude.

SENEX flight on July 3

Observations from IMPROVE, HMS and SENEX identified fire signals on July 3 (ASDTA retrievals were not available), but those signals were missed by the model. In this section, we will use all of evaluation methods addressed above to study potential causes of failure of the model to reproduce fire signals.

At MACA, an IMPROVE site, on July 3 2013, the wind direction at the surface was southeasterly, with no fire hotspots (solid black circle) located upwind of MACA (Fig. 9a). Without any identified hotspots upwind, the model missed fire signals observed at MACA on July 3 2013.

Geosci. Model Dev. Discuss., https://doi.org/10.5194/gmd-2017-207
Manuscript under review for journal Geosci. Model Dev.
Discussion started: 6 November 2017

Flight #0703 was a night mission targeting power plants in Missouri and Arkansas. The flight path is shown in Fig. 9b and is colored by measured CH_3CN concentration. In order to highlight CH_3CH concentrations above 400 ppt in the measurements, CH_3CN concentrations below 400 ppt are represented by black dots. During the flight, 16 measurements of acetonitrile concentration above 400 ppt were observed and the maximum was 3227.9 ppt. These observations were located over northwestern Tennessee and close to the borders of Kentucky, Illinois, Missouri and Arkansas. Except for one observation, the flight altitude was between 500 m and 1000 m.

Enhancements of CO and OC were also measured concurrently with CH_3CN. Figs. 9c and 9d show scatter plots for CH_3CN versus CO and OC, respectively. Measured CH_3CN was highly correlated to both measured CO and OC, with linear correlation coefficients (R^2) of 0.83 and 0.71, respectively. $\Delta CH_3CN/\Delta CO$ ratio is around 2.7 (ppt/ppb), which is consistent with findings of other measurements over California in 2002 when a strong forest fire signal was intercepted by aircraft (de Gouw et al., 2003). $\Delta CH_3CN/\Delta CO$ ratio was around 6.85 (ppt/(mg m^{-3})) which is in the range of biomass burning analyses in MILAGRO (Megacity Initiative Local and Global Research Observations) (Aiken et al., 2010).

Fig. 9e shows model simulated ΔCO with peaks at altitudes below 3000 m. Fire signals showed substantial influences on aircraft measurement at around 5 UTC. However, clear fire signals (between 2 UTC and 3 UTC) were observed based on prior CH_3CN analysis, the model either predicted insufficient fire emission influences or missed it. FMS score on July 3 was 30%. Fig. 9f shows that CMAQ did not predict plumes where the HMS plume analysis exhibited several dense smoke plumes. As NOAA Smoke Text Product (http://www.ssd.noaa.gov/PS/FIRE/DATA/SMOKE) described on its July 03 0501 UTC report:" a smaller very dense patch of remnant smoke, analyzed earlier today over southern Missouri, drifted southward into Arkansas."

The reasons the model missed these fire observations are not clear. Figs. 10, 11a and 11b suggest clues. Fig 10 is a backward trajectory analysis plot for the observations obtained during the SENEX flight on July 3 with CH_3CN measured concentration above 400 ppt. Both transect and flight altitude of the air parcels clearly showed those measurements were most likely influenced by the nearby pollution sources. Fig. 11a illustrates the locations of fire used in the CMAQ simulation. It is noted that hmshysplit.txt is input into BlueSky after HMS quality control (Fig. 1). There were several hotspots around the region where the IMPROVE site MACA is located and where the SENEX flight overpassed. Our fire simulation system might have underestimated smoke emissions from those fires. Other explanation was from Fig. 11b, which illustrated hotspots in hmx.txt. In hmx.txt --- showing every detected fire spots by HMS before quality control. Comparing Fig. 11a with 11b, there were clusters of fire spots in the central U. S. especially in West Tennessee. However, those spots were removed during the HMS quality control process because there were no associated smoke plumes visible. In most of times, those fires were believed to be small sized fires such as from agriculture fires or prescribed burns. For this case, there seem to have been thin clouds overhead and thicker clouds in the vicinity, (http://inventory.ssec.wisc.edu/inventory/image.php?sat=GOES-13&date=2013-07-03&time=16:02&type=Imager&band=1&thefilename=goes13.2013.184.160147.INDX&coverage=CONUS&count=1&offsettz=0), so it would be hard to differentiate smoke form clouds from satellite observations

CONCLUSIONS

In support of the NOAA SENEX field experiment in June-July 2013, simulations were conducted including smoke emissions from fires. In this study, a system accounting for fire emissions in a chemical transport model is described, including a satellite fire detecting system (HMS), a fire emission calculation model (BlueSky), a pre-processing of fire emissions (SMOKE), and simulation over the SENEX domain by

CMAQ. The focus of this work is to qualitatively evaluate the system's capability to capture fire signals identified by multiple observation data sets. These data sets included IMPROVE ground station observations, satellite observations (HMS plume shapefile and ASDTA) and airborne measurements from the SENEX campaign.

For IMPROVE data, potential fire signals were identified by measured potassium concentrations in PM2.5. Fire identifications in CMAQ rely on its predicted ΔCO, the difference between simulations run with and without fire emissions. Three out of four observed fire signals were captured by CMAQ simulations. For HMS smoke plume shapefiles that were manually plotted by analysts to represent the regions impacted by smoke, we used FMS to calculate the percentage of its overlapping with CMAQ predicted smoke plumes. FMS averaged 22% over forty days of the SENEX campaign. In terms of fire smoke impacts on ΔAOD both ASDTA and CMAQ showed similar patterns that were compared with HMS plume shapefile analysis. In terms of measured CH_3CN, a biomass burning plume tracer, both SENEX aircraft in-flight measurements and CMAQ simulations captured signatures of long range transport of fire emissions.

Generally, using HMS-detected fire hotspots and smoke data was useful for predictions of fire impacts and their evaluation. The HMS-BlueSky-SMOKE-CMAQ fire simulation system, which is also used in NAQFC, was able to capture most of the fire signals detected by multiple observations. However, the system failed to identify fire cases on June 17 and July 3, thereby demonstrating two problems with the simulation system. One identified problem is the lack of a dynamical fire lateral boundary condition outside the CONUS domain to represent the inflows of strong fire signals originating from outside the simulation domain. Secondly, the HMS quality control procedure eliminated fire hotspots that were not associated with visible smoke plumes leading to an underestimation.

We were kin on understanding and quantifying the various uncertainties and observational constraints of this study therefore the following rules of thumb were observed: (1) A holistic evaluation approach was adopted so that the fire model was interpreted as a single entity to avoid being bogged down by uncertainties specific to the different components in the modeling system, (2) Analysis conclusion applicable to the entire simulation period was drawn so that the episodic characteristics of the cases embedded in the simulation were averaged and generalized. This had advantages and disadvantages. The advantages outweighed the disadvantages in terms of the functionality and consistency of the forecasting application endpoints of NAQFC, (3) We took advantage of the multiple perspectives of the observation systems that offered a wide spectrum of temporal and spatial variabilities intrinsic to the systems, and (4) We were intentional to be conservative in discarding data so that we maximized the sampling pool for statistical analysis and avoided unwittingly discarding poorly simulated cases, good out-layers, and weak sparse but accurate signals.

Quantitative evaluation of fire emissions and their subsequent influences on ozone and particulate matter in this fire and smoke prediction system is challenging. Future work includes applying these findings to the NAQFC and improving the modeling system's capabilities to simulate fires accurately.

Code Availability

The source code used in this study is available online at http://www.nco.ncep.noaa.gov/pmb/codes/nwprod/cmaq.v5.0.2.

Acknowledgements & disclaimer

This work was partially funded by the NASA Air Quality Applied Sciences Team (AQAST), project grant NNH14AX881. The authors are thankful to Dr. Joost De Gouw and Dr. Martin G. Graus of the Earth

System Research Laboratory, NOAA for sharing the SENEX campaign data used in this study. Although this work has been reviewed by the Air Resources Laboratory, NOAA and approved for publication it does not necessarily reflect their policies or views.

Figures:

Figure 1, Fire emission calculation and smoke plume simulation algorithm.

Figure 2, in 4km SENEX domain, (a): the contribution (%) of CO emission from fires occurred inside the SENEX domain; (b): the contribution (%) of CO flux flowing into the SENEX domain from its boundary caused by fires burning outside the SENEX domain but inside the CONUS domain.

Figure 3, simulated ΔCO (ppb) extracted along SENEX flight path.

Figure 4, ΔCO (>2.0 ppb) simulated in SENEX domain on June 24, 2013. The solid circle is detected fire hotspots by HMS. The open triangle represents IMPROVE sites.

Figure 5, FMS (Figure of Merits in Space) (%) from June 11 to July 19 in 2013 during SENXE experiment.

Figure 6, HMS observed plume shape versus CMAQ predicted plume shape on (a): July 6 2013; (b) June 17, 2013; (c), HMS observed plume shape (white) and fire hotspots (red) on June 17, 2013.

Figure 7, GOES detected AOD influenced by fires using ASDTA diagnose method on (a): June 14, 2013; (d) June 25, 2013; ΔAOD (withfire – nofire) simulated in CMAQ on (b): June 14, 2013; (e) June 25, 2013; HMS observed plume shape and fire hotspots on (c): June 14, 2013; (f) June 25, 2013.

Figure 8, CMAQ simulated ΔCO vertical distributions along SENEX flight transect on (a): June 16, 2013; (b): July 10, 2013; Two color bars represent observed CH_3CN concentration (rectangle bar => ppt) and simulated ΔCO concentration (fan bar => ppb), respectively.

Figure 9, plots for July 3 2013 case, (a): IMPROVE; (b): the flight path of SENEX #0703 colored by measured CH_3CN concentration (ppt); (c): CH_3CN (ppt) vs CO (ppb); (d): CH_3CN (ppt) vs AMS_Org (mg m^{-3}); (e): CMAQ simulated ΔCO vertical distributions along flight transect; (f): HMS observed plume shape versus CMAQ prediction.

Figure 10, a backward trajectory analysis for the observations obtained during the SENEX flight on July 03 with CH_3CN measured concentration above 400 ppt.

Figure 11, detected fire hotspots on July 03, 2013 (a): hmxhysplit.txt; (b): hmx.txt.

Geosci. Model Dev. Discuss., https://doi.org/10.5194/gmd-2017-207
Manuscript under review for journal Geosci. Model Dev.
Discussion started: 6 November 2017

Geoscientific Model Development
Discussions
Open Access
EGU

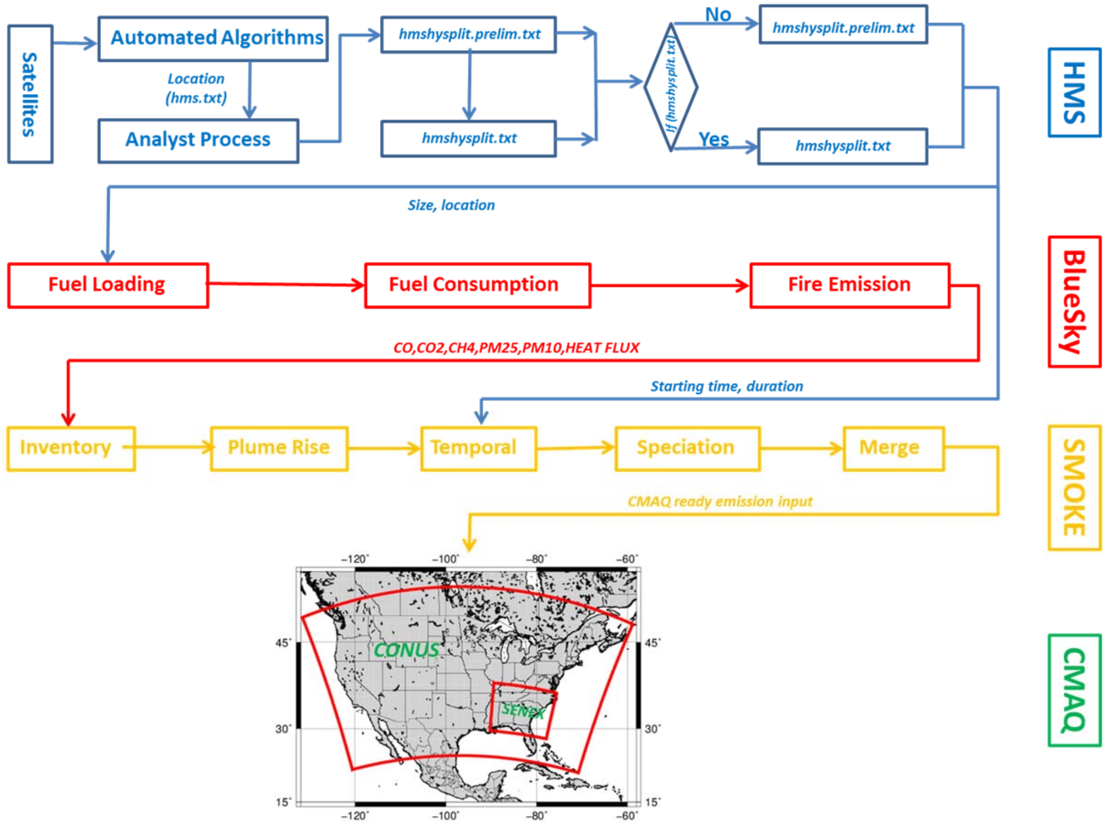

Figure 1: Fire emission calculation and smoke plume simulation algorithm

Geosci. Model Dev. Discuss., https://doi.org/10.5194/gmd-2017-207
Manuscript under review for journal Geosci. Model Dev.
Discussion started: 6 November 2017

Geoscientific Model Development
Discussions
Open Access

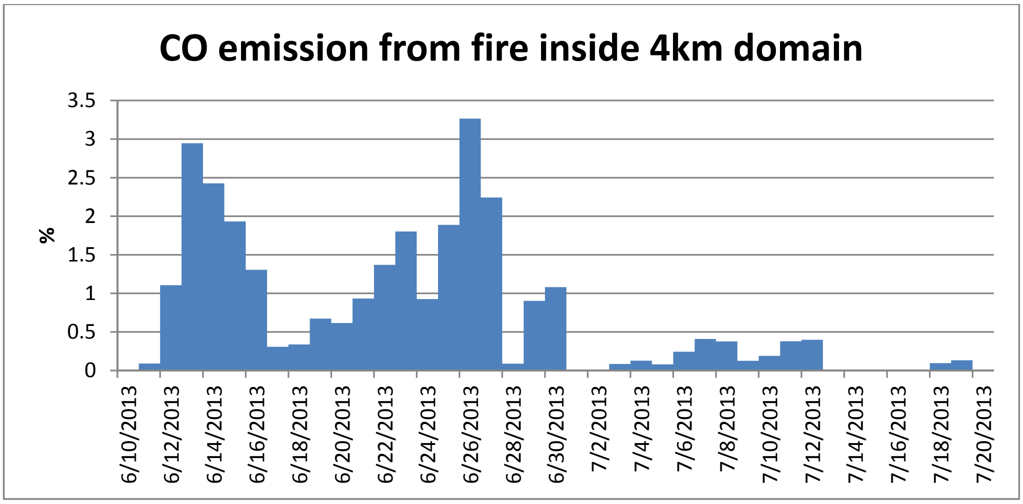

Figure 2a

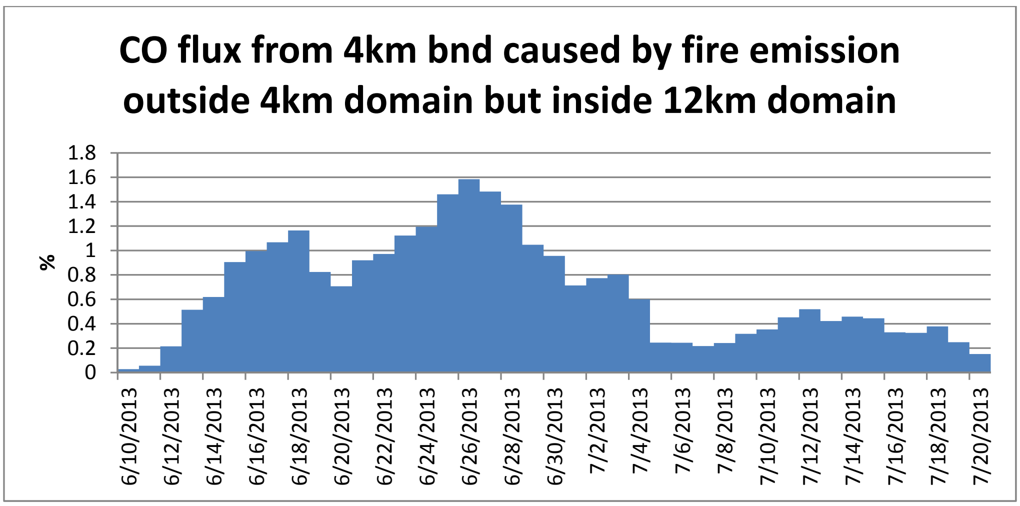

Figure 2b

Geosci. Model Dev. Discuss., https://doi.org/10.5194/gmd-2017-207
Manuscript under review for journal Geosci. Model Dev.
Discussion started: 6 November 2017

Geoscientific Model Development Discussions

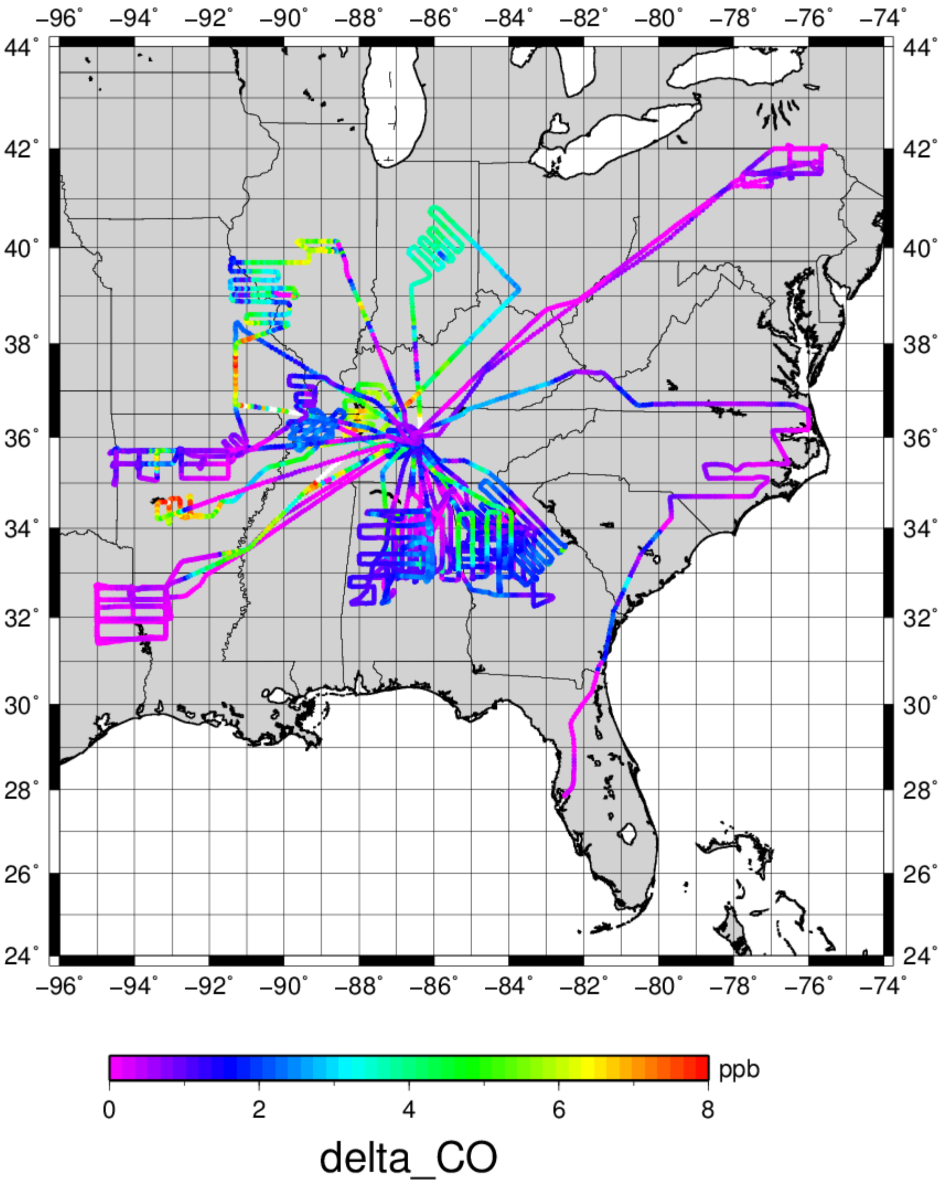

509

510 **Figure 3: simulated ΔCO (ppb) extracted along SENEX flight path**

511

Geosci. Model Dev. Discuss., https://doi.org/10.5194/gmd-2017-207
Manuscript under review for journal Geosci. Model Dev.
Discussion started: 6 November 2017

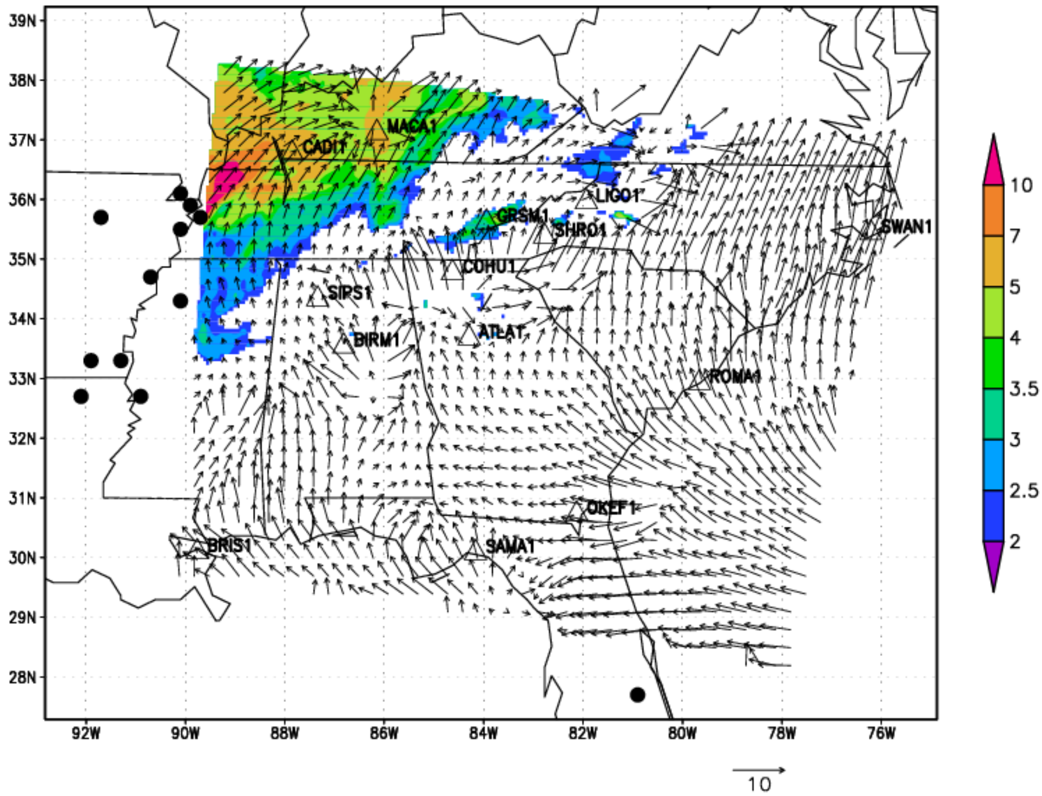

Figure 4: ΔCO (>2.0ppb) simulated in SENEX domain on June 24, 2013

Geosci. Model Dev. Discuss., https://doi.org/10.5194/gmd-2017-207
Manuscript under review for journal Geosci. Model Dev.
Discussion started: 6 November 2017

Geoscientific Model Development Discussions
Open Access
EGU

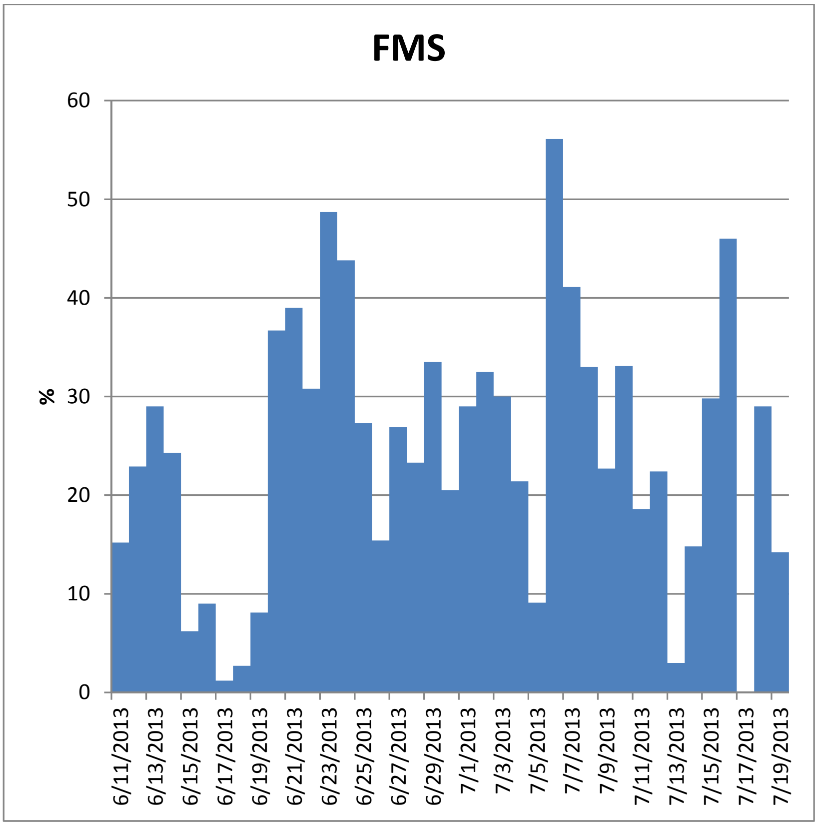

Figure 5: FMS (Figure of Merits in Space) (%) from June 11 to July 19 in 2013 during SENXE experiment

Geosci. Model Dev. Discuss., https://doi.org/10.5194/gmd-2017-207
Manuscript under review for journal Geosci. Model Dev.
Discussion started: 6 November 2017

Geoscientific Model Development Discussions
Open Access EGU

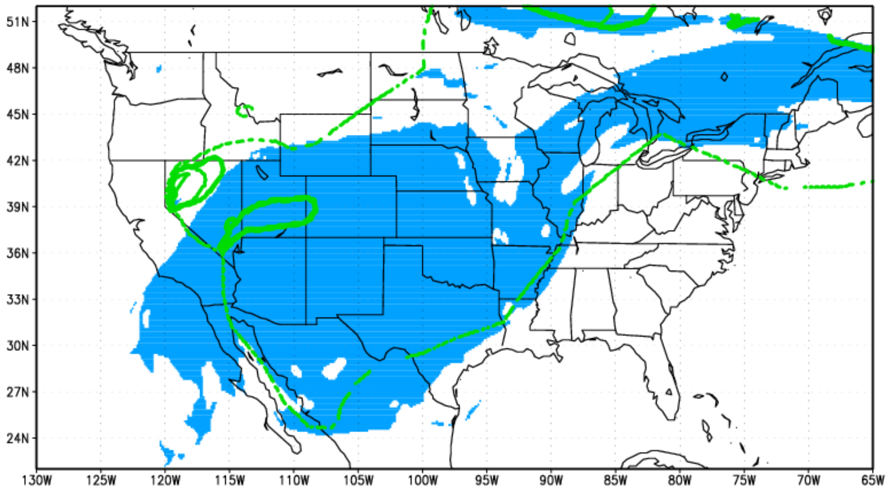

Figure 6a: HMS observed plume shape versus CMAQ predicted plume shape on July 6, 2013

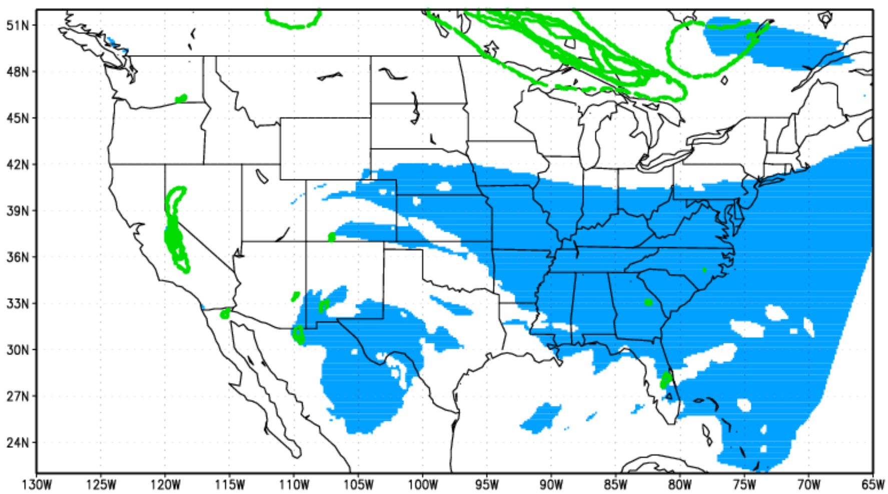

Figure 6b: on June 17 2013

Geosci. Model Dev. Discuss., https://doi.org/10.5194/gmd-2017-207
Manuscript under review for journal Geosci. Model Dev.
Discussion started: 6 November 2017

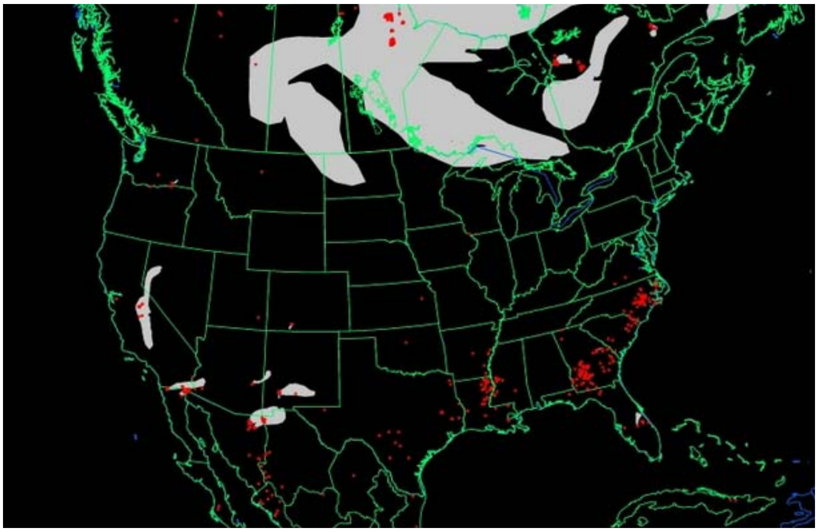

Figure 6c: HMS detected fire hotspots (red) and smoke plume shapes (white) on June 17, 2013 (http://ready.arl.noaa.gov/data/archives/fires/national/arcweb)

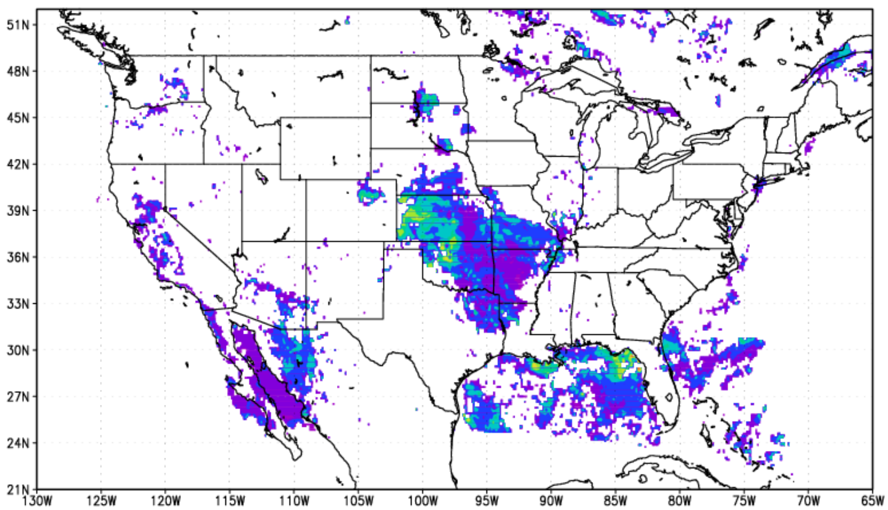

Figure 7a: GOES detected AOD influenced by fires using ASDTA diagnose method on June 14, 2013

Geosci. Model Dev. Discuss., https://doi.org/10.5194/gmd-2017-207
Manuscript under review for journal Geosci. Model Dev.
Discussion started: 6 November 2017

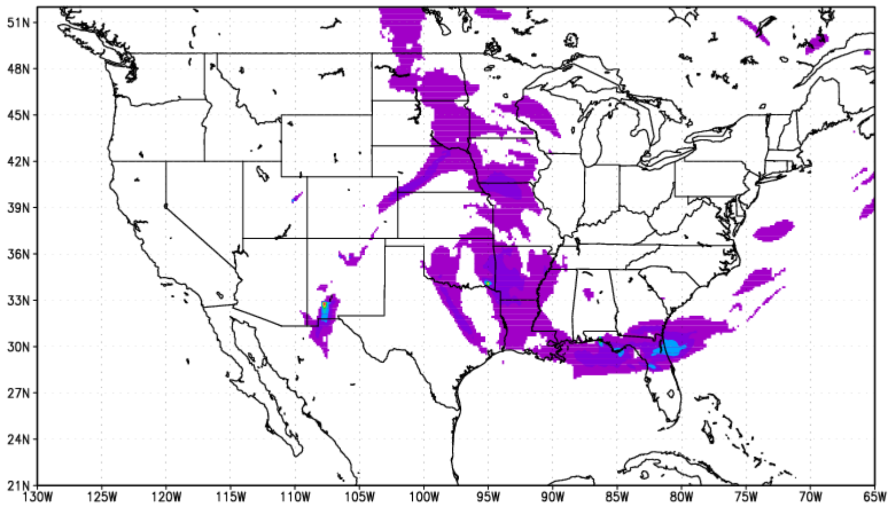

Figure 7b: ΔAOD (withfire – nofire) simulated in CMAQ on June 14, 2013

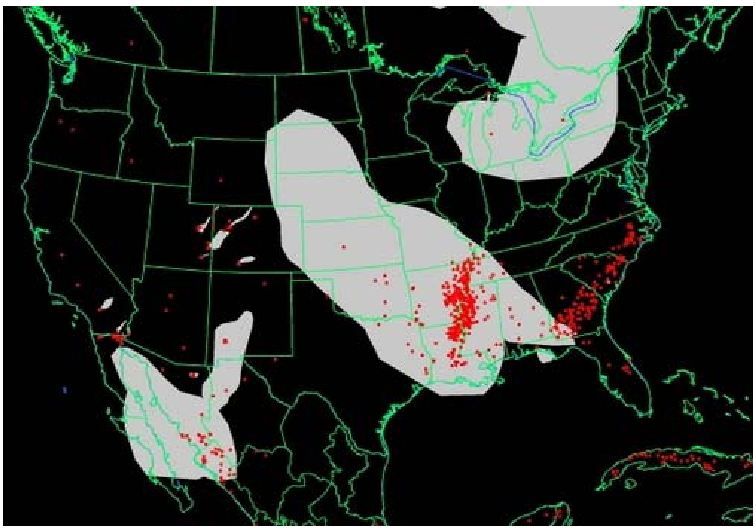

Figure 7c: HMS detected fire hot spots and smoke plume shapes on June 14, 2013 (http://ready.arl.noaa.gov/data/archives/fires/national/arcweb)

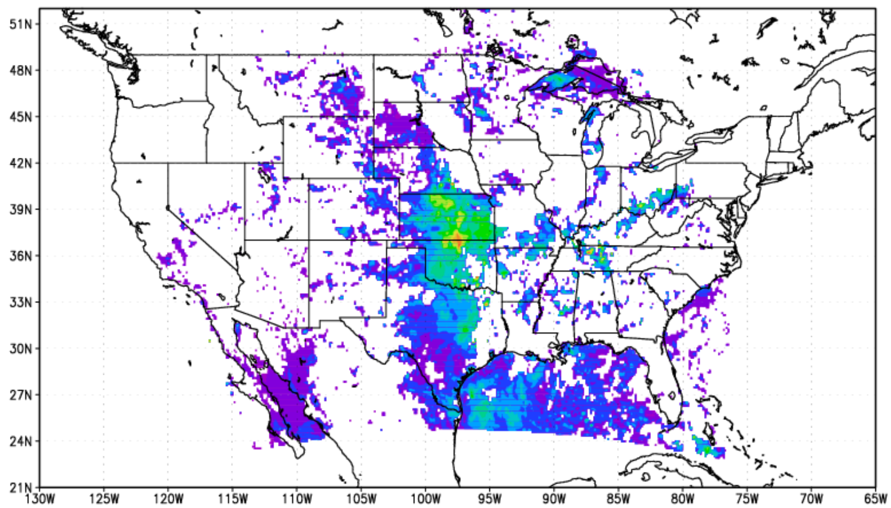

Figure 7d: GOES detected AOD influenced by smoke plumes using ASDTA on June 25, 2013

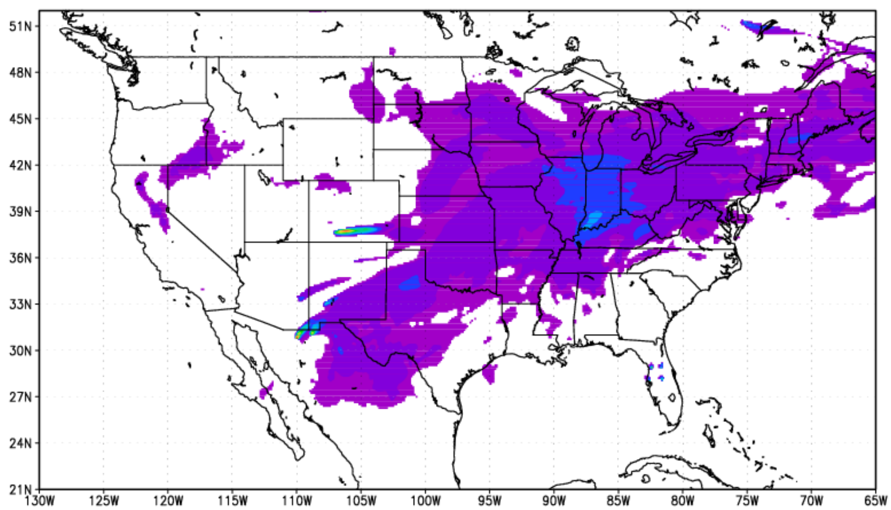

Figure 7e: ΔAOD (withfire – nofire) simulated in CMAQ on June 25, 2013

Geosci. Model Dev. Discuss., https://doi.org/10.5194/gmd-2017-207
Manuscript under review for journal Geosci. Model Dev.
Discussion started: 6 November 2017

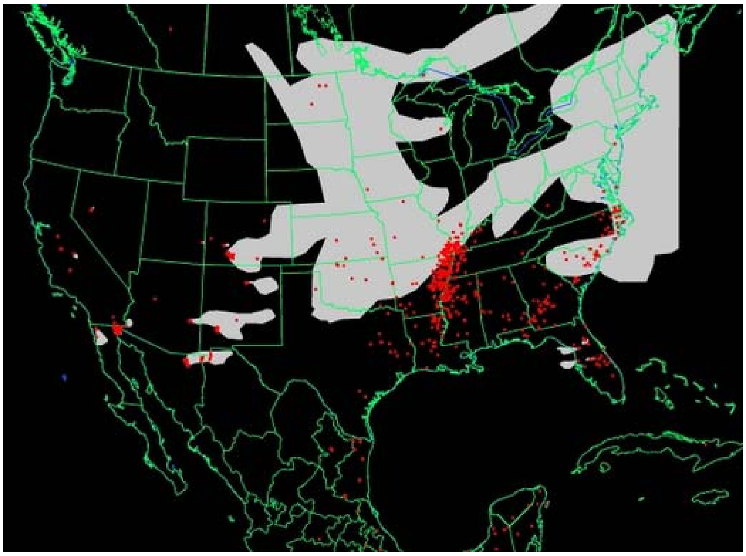

Figure 7f: HMS detected fire hot spots and smoke plume shapes on June 25, 2013 (http://ready.arl.noaa.gov/data/archives/fires/national/arcweb)

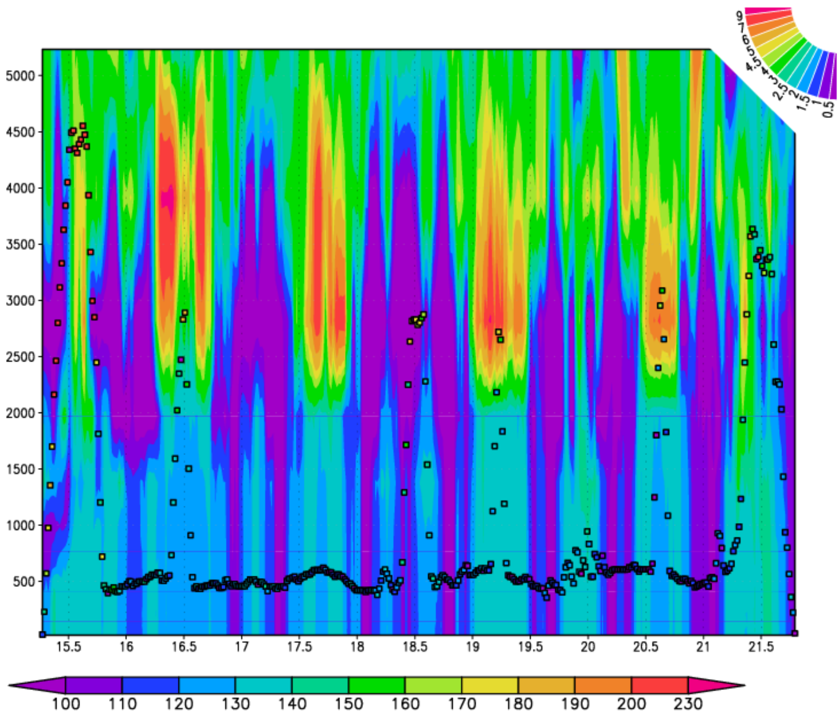

Figure 8a: CMAQ simulated ΔCO (ppb) vertical distributions along flight transect on June 16, 2013.

Geosci. Model Dev. Discuss., https://doi.org/10.5194/gmd-2017-207
Manuscript under review for journal Geosci. Model Dev.
Discussion started: 6 November 2017

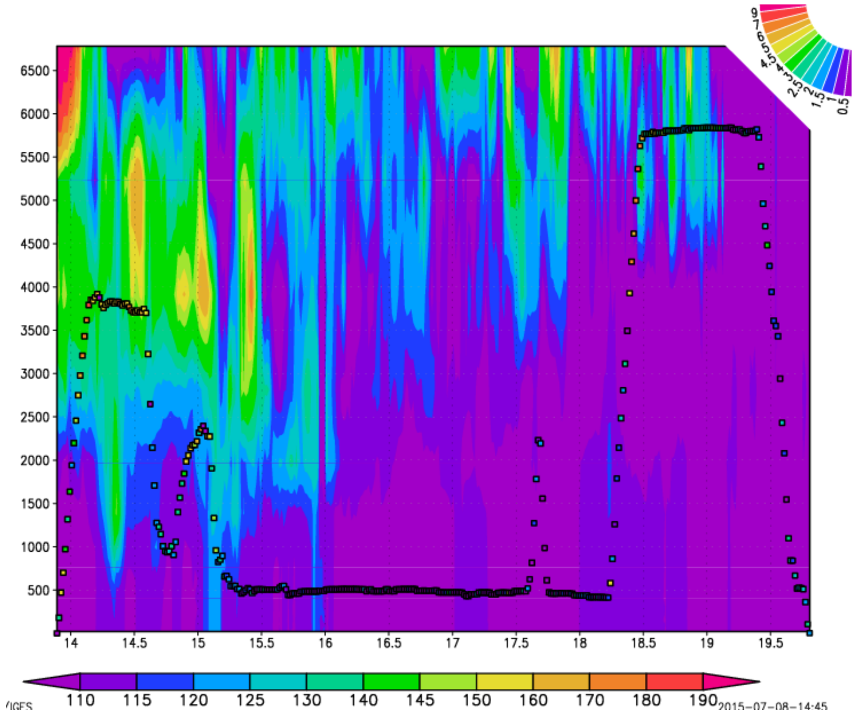

Figure 8b: CMAQ simulated ΔCO (ppb) vertical distributions along flight transect on July 10, 2013

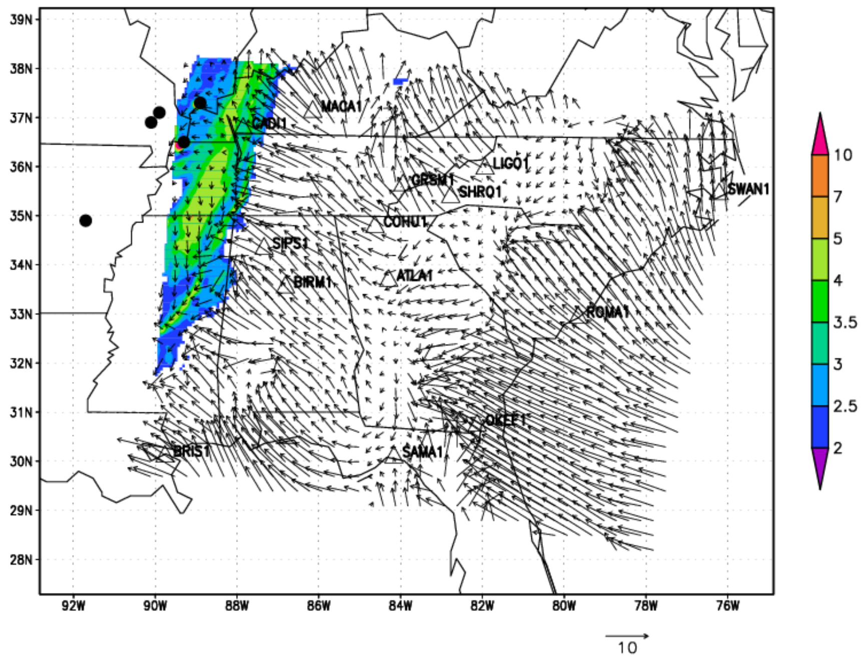

Figure 9a: ΔCO (>2.0ppb) simulated in SENEX domain on July 03, 2013

Geosci. Model Dev. Discuss., https://doi.org/10.5194/gmd-2017-207
Manuscript under review for journal Geosci. Model Dev.
Discussion started: 6 November 2017

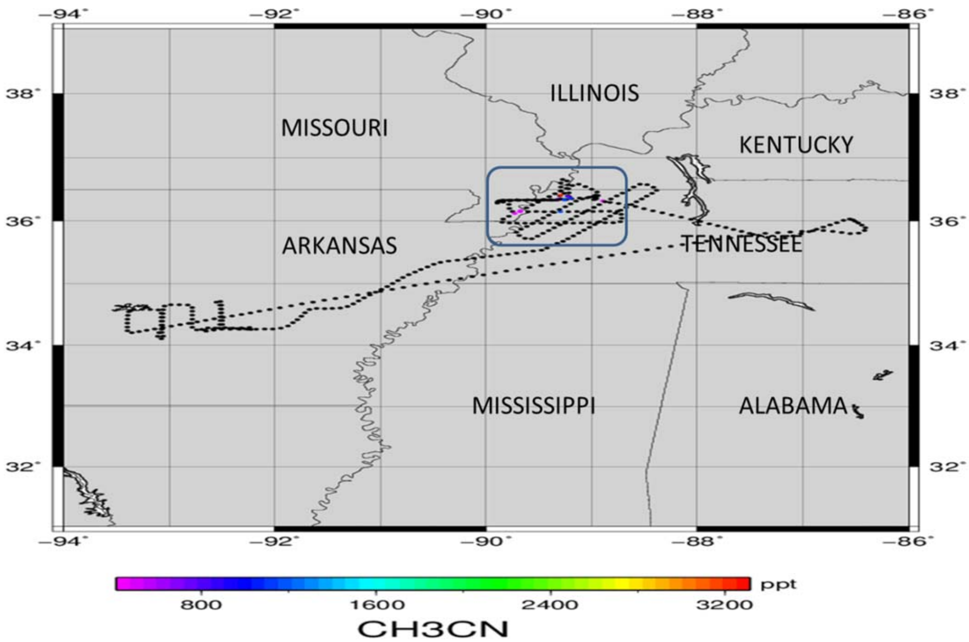

Figure 9b: the flight path of SENEX #0703, colored by measured CH3CN concentration (ppt)

Geosci. Model Dev. Discuss., https://doi.org/10.5194/gmd-2017-207
Manuscript under review for journal Geosci. Model Dev.
Discussion started: 6 November 2017

Geoscientific Model Development
Discussions
Open Access
EGU

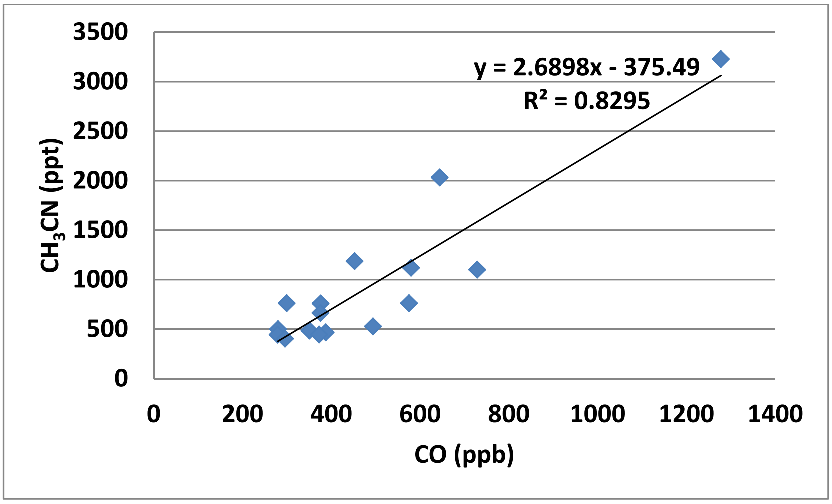

Figure 9c: CH_3CN (ppt) vs CO (ppb)

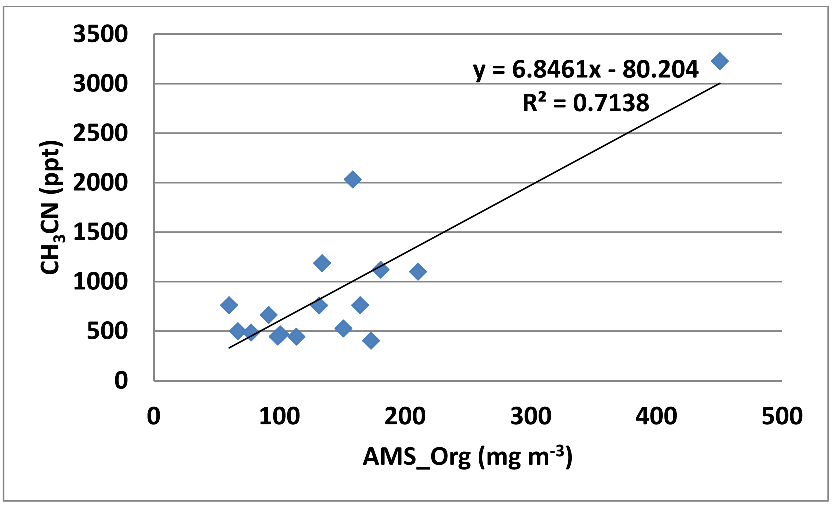

Figure 9d: CH_3CN (ppt) vs AMS_Org (mg m^{-3})

Geosci. Model Dev. Discuss., https://doi.org/10.5194/gmd-2017-207
Manuscript under review for journal Geosci. Model Dev.
Discussion started: 6 November 2017

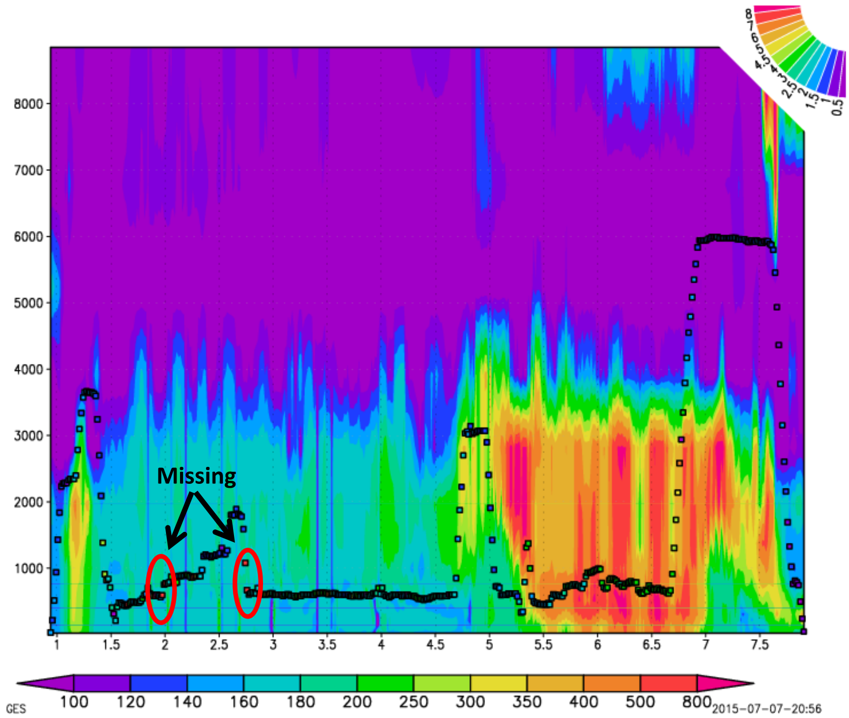

611

612 **Figure 9e: CMAQ simulated ΔCO (ppb) vertical distributions along flight transect on July 03, 2013**

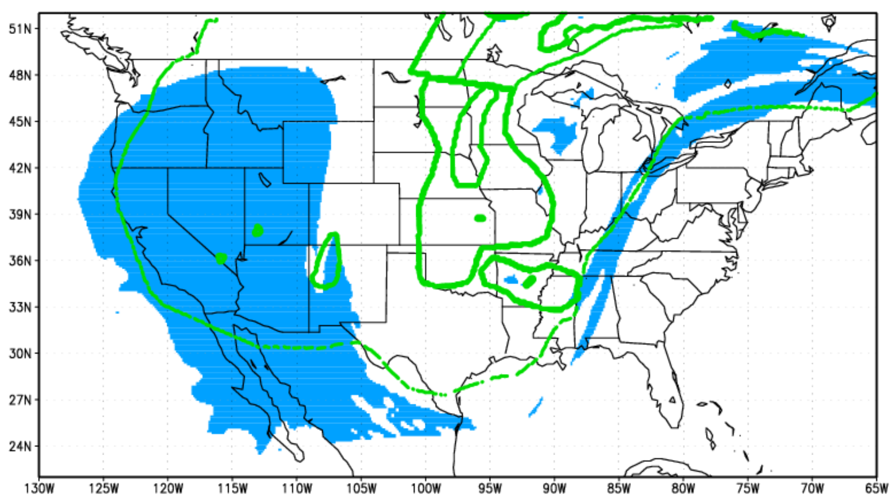

613

614 **Figure 9f: HMS plume shape versus CMAQ predictions on July 03, 2013**

615

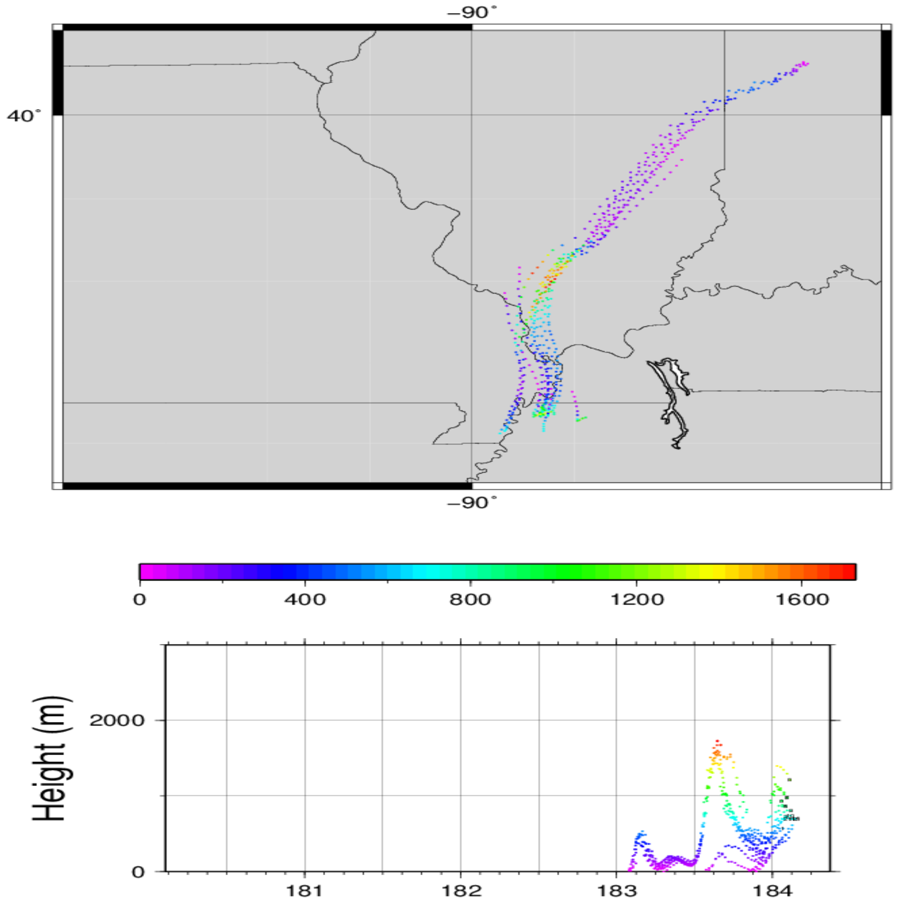

616

617 **Figure 10, a backward trajectory analysis for the observations obtained during the SENEX flight on July**
618 **03 with CH_3CN measured concentration above 400 ppt.**

Geosci. Model Dev. Discuss., https://doi.org/10.5194/gmd-2017-207
Manuscript under review for journal Geosci. Model Dev.
Discussion started: 6 November 2017

Geoscientific Model Development Discussions
Open Access

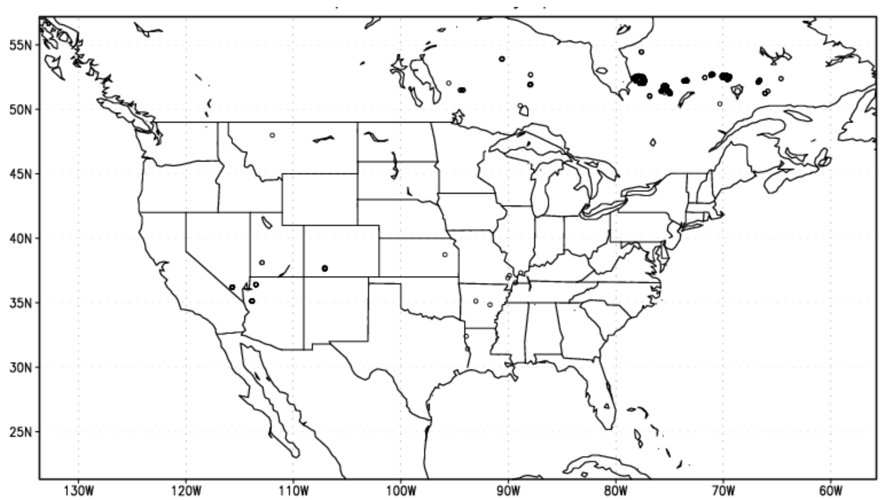

Figure 11a: fire hotspots in hmxhysplit.txt on July 03, 2013

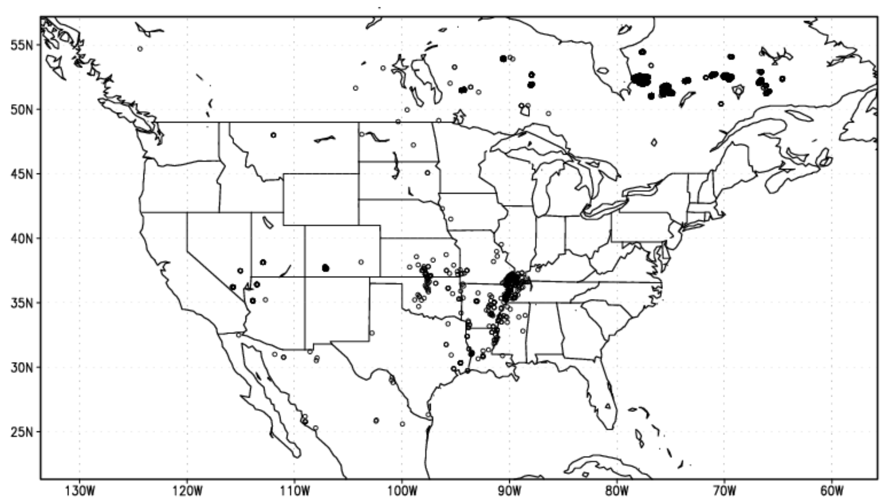

Figure 11b: fire hotspots in hmx.txt on July 03, 2013

Geosci. Model Dev. Discuss., https://doi.org/10.5194/gmd-2017-207
Manuscript under review for journal Geosci. Model Dev.
Discussion started: 6 November 2017

Geoscientific Model Development
Discussions
Open Access
EGU

Tables:

Table 1: observed and simulated CO (ppb) during NOAA SENEX experiment

ALT (m)	NUMS	OBS	OBS_MAX	Mod_withfire	Mod_nofire	ΔCO
<500	166	128.93±38.51	319.55	108.70±21.37	107.16±20.34	1.54
500~1000	3565	146.19±44.39	1277.97	108.39±19.82	106.50±18.86	1.88
1000~1500	793	125.41±28.09	299.64	100.11±15.63	98.49±14.67	1.62
1500~2000	306	119.68±23.99	265.29	100.75±17.04	99.08±15.89	1.67
2000~2500	219	111.48±19.98	286.22	99.88±17.95	98.37±16.92	1.51
2500~3000	209	111.84±19.79	295.79	97.43±12.21	95.87±11.15	1.56
3000~3500	181	109.31±16.66	197.94	89.34±12.09	88.13±11.06	1.21
3500~4000	195	110.78±14.36	140.42	92.11±10.73	90.25±9.62	1.86
4000~5000	369	89.82±19.09	138.04	80.36±10.15	79.17±9.14	1.19
5000~6000	354	102.26±22.37	209.20	78.12±7.64	76.82±6.28	1.30
6000~7000	85	87.53±17.88	115.32	73.35±4.71	70.58±2.45	2.77

Table 2: identified fire signals from IMPROVE measurements during SENEX experiment

Site	Date	Concentrations (ug m^{-3})						Concentration/Average						Ratio	
		EC	OC	K	SOIL	NO_3^-	SO_4^{2-}	EC	OC	K	SOIL	NO_3^-	SO_4^{2-}	BC/OC	K/BC
COHU	0621	0.28	2.10	0.05	0.22	0.13	2.61	1.4	1.46	1.42	0.39	0.84	1.28	0.1331	0.1933
MACA	0624	0.45	2.34	0.09	0.26	0.24	2.76	1.85	1.58	1.82	0.48	1.19	1.24	0.1929	0.1973
MACA	0703	0.33	2.32	0.08	0.16	0.29	2.11	1.35	1.57	1.73	0.29	1.43	0.94	0.1423	0.2554
BRIS	0703	0.24	0.98	0.21	0.31	0.11	2.63	1.49	1.28	2.79	0.13	0.35	1.36	0.2458	0.8851
GRSM	0621	0.25	1.56	0.05	0.24	0.13	2.52	1.36	1.45	1.24	0.49	0.99	1.42	0.1596	0.1979

References:

Achtemeier, G. L., S. A. Goodrick, Y. Q. Liu, F. Garcia-Menendez, Y. T. Hu, and M. T. Odman. Modeling Smoke Plume-Rise and Dispersion from Southern United States Prescribed Burns with Daysmoke, *Atmosphere*, 2: 358-88. doi:10.3390/atmos2030358, 2011.

Aiken, A. C., B. de Foy, C. Wiedinmyer, P. F. DeCarlo, I. M. Ulbrich, M. N. Wehrli, S. Szidat, A. S. H. Prevot, J. Noda, L. Wacker, R. Volkamer, E. Fortner, J. Wang, A. Laskin, V. Shutthanandan, J. Zheng, R. Zhang, G. Paredes-Miranda, W. P. Arnott, L. T. Molina, G. Sosa, X. Querol, and J. L. Jimenez. Mexico city aerosol analysis during MILAGRO using high resolution aerosol mass spectrometry at the urban supersite (T0) - Part 2: Analysis of the biomass burning contribution and the non-fossil carbon fraction, *Atmospheric Chemistry and Physics*, 10: 5315-41. doi:10.5194/acp-10-5315-2010, 2010.

Alvarado, M. J., C. R. Lonsdale, R. J. Yokelson, S. K. Akagi, H. Coe, J. S. Craven, E. V. Fischer, G. R. McMeeking, J. H. Seinfeld, T. Soni, J. W. Taylor, D. R. Weise, and C. E. Wold. Investigating the links between ozone and organic aerosol chemistry in a biomass burning plume from a prescribed fire in California chaparral, *Atmospheric Chemistry and Physics*, 15: 6667-88. doi:10.5194/acp-15-6667-2015, 2015.

Baker, K. R., M. C. Woody, G. S. Tonnesen, W. Hutzell, H. O. T. Pye, M. R. Beaver, G. Pouliot, and T. Pierce. Contribution of regional-scale fire events to ozone and PM2.5 air quality estimated by photochemical modeling approaches, *Atmospheric Environment*, 140: 539-54. doi:10.1016/j.atmosenv.2016.06.032, 2016.

Carlton, A. G., P. V. Bhave, S. L. Napelenok, E. D. Edney, G. Sarwar, R. W. Pinder, G. A. Pouliot, and M. Houyoux. Model Representation of Secondary Organic Aerosol in CMAQv4.7, *Environmental Science & Technology*, 44: 8553-60. doi:10.1021/es100636q, 2010.

Chai, T., H. C. Kim, P. Lee, D. Tong, L. Pan, Y. Tang, J. Huang, J. McQueen, M. Tsidulko, and I. Stajner. Evaluation of the United States National Air Quality Forecast Capability experimental real-time predictions in 2010 using Air Quality System ozone and NO2 measurements, *Geoscientific Model Development*, 6: 1831-50. doi:10.5194/gmd-6-1831-2013, 2013.

Davis, A. Y., R. Ottmar, Y. Q. Liu, S. Goodrick, G. Achtemeier, B. Gullett, J. Aurell, W. Stevens, R. Greenwald, Y. T. Hu, A. Russell, J. K. Hiers, and M. T. Odman. Fire emission uncertainties and their effect on smoke dispersion predictions: a case study at Eglin Air Force Base, Florida, USA, *International Journal of Wildland Fire*, 24: 276-85. doi:10.1071/wf13071, 2015.

de Gouw, J. A., C. Warneke, D. D. Parrish, J. S. Holloway, M. Trainer, and F. C. Fehsenfeld. Emission sources and ocean uptake of acetonitrile (CH3CN) in the atmosphere, *Journal of Geophysical Research-Atmospheres*, 108. doi:10.1029/2002jd002897, 2003.

DeBell, L. J., R. W. Talbot, J. E. Dibb, J. W. Munger, E. V. Fischer, and S. E. Frolking. A major regional air pollution event in the northeastern United States caused by extensive forest fires in Quebec, Canada, *Journal of Geophysical Research-Atmospheres*, 109. doi:10.1029/2004jd004840, 2004.

Delfino, R. J., S. Brummel, J. Wu, H. Stern, B. Ostro, M. Lipsett, A. Winer, D. H. Street, L. Zhang, T. Tjoa, and D. L. Gillen. The relationship of respiratory and cardiovascular hospital admissions to the southern California wildfires of 2003, *Occupational and Environmental Medicine*, 66: 189-97. doi:10.1136/oem.2008.041376, 2009.

Draxier, R. R., and G. D. Hess. An overview of the HYSPLIT_4 modelling system for trajectories, dispersion and deposition, *Australian Meteorological Magazine*, 47: 295-308. 1998.

Dreessen, J., J. Sullivan, and R. Delgado. Observations and impacts of transported Canadian wildfire smoke on ozone and aerosol air quality in the Maryland region on June 9-12, 2015, *Journal of the Air & Waste Management Association*, 66: 842-62. doi:10.1080/10962247.2016.1161674, 2016.

Drury, S. A., N. Larkin, T. T. Strand, S. M. Huang, S. J. Strenfel, E. M. Banwell, T. E. O'Brien, and S. M. Raffuse. INTERCOMPARISON OF FIRE SIZE, FUEL LOADING, FUEL CONSUMPTION, AND SMOKE EMISSIONS ESTIMATES ON THE 2006 TRIPOD FIRE,WASHINGTON, USA, *Fire Ecology*, 10: 56-83. doi:10.4996/fireecology.1001056, 2014.

Eatough, D. J., D. A. Eatough, L. Lewis, and E. A. Lewis. Fine particulate chemical composition and light extinction at Canyonlands National Park using organic particulate material concentrations obtained with a multisystem, multichannel diffusion denuder sampler, *Journal of Geophysical Research-Atmospheres*, 101: 19515-31. doi:10.1029/95jd01385, 1996.

Erbrink, H. J. PLUME RISE IN DIFFERENT ATMOSPHERES - A PRACTICAL SCHEME AND SOME COMPARISONS WITH LIDAR MEASUREMENTS, *Atmospheric Environment*, 28: 3625-36. doi:10.1016/1352-2310(94)00197-s, 1994.

Giglio, L., J. Descloitres, C. O. Justice, and Y. J. Kaufman. An enhanced contextual fire detection algorithm for MODIS, *Remote Sensing of Environment*, 87: 273-82. doi:10.1016/s0034-4257(03)00184-6, 2003.

Hamm, S., and P. Warneck. THE INTERHEMISPHERIC DISTRIBUTION AND THE BUDGET OF ACETONITRILE IN THE TROPOSPHERE, *Journal of Geophysical Research-Atmospheres*, 95: 20593-606. doi:10.1029/JD095iD12p20593, 1990.

Hardy, C. C., and C. E. Hardy. Fire danger rating in the United States of America: an evolution since 1916, *International Journal of Wildland Fire*, 16: 217-31. doi:10.1071/wf06076, 2007.

Herron-Thorpe, F. L., G. H. Mount, L. K. Emmons, B. K. Lamb, D. A. Jaffe, N. L. Wigder, S. H. Chung, R. Zhang, M. D. Woelfle, and J. K. Vaughan. Air quality simulations of wildfires in the Pacific Northwest evaluated with surface and satellite observations during the summers of 2007 and 2008, *Atmospheric Chemistry and Physics*, 14: 12533-51. doi:10.5194/acp-14-12533-2014, 2014.

Holzinger, R., C. Warneke, A. Hansel, A. Jordan, W. Lindinger, D. H. Scharffe, G. Schade, and P. J. Crutzen. Biomass burning as a source of formaldehyde, acetaldehyde, methanol, acetone, acetonitrile, and hydrogen cyanide, *Geophysical Research Letters*, 26: 1161-64. doi:10.1029/1999gl900156, 1999.

Hu, X. F., C. Yu, D. Tian, M. Ruminski, K. Robertson, L. A. Waller, and Y. Liu. Comparison of the Hazard Mapping System (HMS) fire product to ground-based fire records in Georgia, USA, *Journal of Geophysical Research-Atmospheres*, 121: 2901-10. doi:10.1002/2015jd024448, 2016.

Huang, J., J. McQueen, J. Wilczak, I. Djalalova, I. Stajner, P. Shafran, D. Allured, P. Lee, L. Pan, D. Tong, H. Huang, G. DiMego, S. Upadhayay, and L. Monache. Improving NOAA NAQFC PM2.5 predictions with a bias correction approach, *Wea. Forecasting*. doi:10.1175/WAF-D-16-0118.1, 2016.

Jaffe, D. A., N. Wigder, N. Downey, G. Pfister, A. Boynard, and S. B. Reid. Impact of Wildfires on Ozone Exceptional Events in the Western US, *Environmental Science & Technology*, 47: 11065-72. doi:10.1021/es402164f, 2013.

Johnston, F. H., S. B. Henderson, Y. Chen, J. T. Randerson, M. Marlier, R. S. DeFries, P. Kinney, Dmjs Bowman, and M. Brauer. Estimated Global Mortality Attributable to Smoke from Landscape Fires, *Environmental Health Perspectives*, 120: 695-701. doi:10.1289/ehp.1104422, 2012.

Justice, C. O., L. Giglio, S. Korontzi, J. Owens, J. T. Morisette, D. Roy, J. Descloitres, S. Alleaume, F. Petitcolin, and Y. Kaufman. The MODIS fire products, *Remote Sensing of Environment*, 83: 244-62. doi:10.1016/s0034-4257(02)00076-7, 2002.

Knorr, W., V. Lehsten, and A. Arneth. Determinants and predictability of global wildfire emissions, *Atmospheric Chemistry and Physics*, 12: 6845-61. doi:10.5194/acp-12-6845-2012, 2012.

Larkin, N. K., S. M. O'Neill, R. Solomon, S. Raffuse, T. Strand, D. C. Sullivan, C. Krull, M. Rorig, J. L. Peterson, and S. A. Ferguson. The BlueSky smoke modeling framework, *International Journal of Wildland Fire*, 18: 906-20. doi:10.1071/wf07086, 2009.

Lee, Pius, Jeffery McQueen, Ivanka Stajner, Jianping Huang, Li Pan, Daniel Tong, Hyuncheol Kim, Youhua Tang, Shobha Kondragunta, and Mark Ruminski. NAQFC developmental forecast guidance for fine particulate matter (PM2. 5), *Weather and Forecasting*, 32: 343-60. doi:10.1175/waf-d-15-0163.1, 2017.

Li, Z., S. Nadon, and J. Cihlar. Satellite-based detection of Canadian boreal forest fires: development and application of the algorithm, *International Journal of Remote Sensing*, 21: 3057-69. doi:10.1080/01431160050144956, 2000.

Malm, W. C., B. A. Schichtel, M. L. Pitchford, L. L. Ashbaugh, and R. A. Eldred. Spatial and monthly trends in speciated fine particle concentration in the United States, *Journal of Geophysical Research-Atmospheres*, 109. doi:10.1029/2003jd003739, 2004.

Neuman, J. A., M. Trainer, S. S. Brown, K. E. Min, J. B. Nowak, D. D. Parrish, J. Peischl, I. B. Pollack, J. M. Roberts, T. B. Ryerson, and P. R. Veres. HONO emission and production determined from airborne measurements over the Southeast US, *Journal of Geophysical Research-Atmospheres*, 121: 9237-50. doi:10.1002/2016jd025197, 2016.

Pan, L., D. Tong, P. Lee, H. C. Kim, and T. F. Chai. Assessment of NOx and O-3 forecasting performances in the US National Air Quality Forecasting Capability before and after the 2012 major emissions updates, *Atmospheric Environment*, 95: 610-19. doi:10.1016/j.atmosenv.2014.06.020, 2014.

Pavlovic, R., J. Chen, K. Anderson, M. D. Moran, P. A. Beaulieu, D. Davignon, and S. Cousineau. The FireWork air quality forecast system with near-real-time biomass burning emissions: Recent developments and evaluation of performance for the 2015 North American wildfire season, *Journal of the Air & Waste Management Association*, 66: 819-41. doi:10.1080/10962247.2016.1158214, 2016.

Prados, A. I., S. Kondragunta, P. Ciren, and K. R. Knapp. GOES Aerosol/Smoke product (GASP) over North America: Comparisons to AERONET and MODIS observations, *Journal of Geophysical Research-Atmospheres*, 112. doi:10.1029/2006jd007968, 2007.

Prins, E. M., and W. P. Menzel. GEOSTATIONARY SATELLITE DETECTION OF BIOMASS BURNING IN SOUTH-AMERICA, *International Journal of Remote Sensing*, 13: 2783-99. 1992.

Rappold, A. G., S. L. Stone, W. E. Cascio, L. M. Neas, V. J. Kilaru, M. S. Carraway, J. J. Szykman, A. Ising, W. E. Cleve, J. T. Meredith, H. Vaughan-Batten, L. Deyneka, and R. B. Devlin. Peat Bog Wildfire Smoke Exposure in Rural North Carolina Is Associated with Cardiopulmonary Emergency Department Visits Assessed through Syndromic Surveillance, *Environmental Health Perspectives*, 119: 1415-20. doi:10.1289/ehp.1003206, 2011.

Reid, J. S., R. Koppmann, T. F. Eck, and D. P. Eleuterio. A review of biomass burning emissions part II: intensive physical properties of biomass burning particles, *Atmospheric Chemistry and Physics*, 5: 799-825. 2005.

Rolph, G. D., R. R. Draxler, A. F. Stein, A. Taylor, M. G. Ruminski, S. Kondragunta, J. Zeng, H. C. Huang, G. Manikin, J. T. McQueen, and P. M. Davidson. Description and Verification of the NOAA Smoke Forecasting System: The 2007 Fire Season, *Weather and Forecasting*, 24: 361-78. doi:10.1175/2008waf2222165.1, 2009.

Ruminski, M., and S. Kondragunta. Monitoring fire and smoke emissions with the hazard mapping system - art. no. 64120B. in F. Kogan, S. Habib, V. S. Hegde and M. Matsuoka (eds.), *Disaster Forewarning Diagnostic Methods and Management*. 2006.

Ruminski, M., J. Simko, J. Kibler, S. Kondragunta, R. Draxler, P. Davidson, and P. Li. Use of multiple satellite sensors in NOAA's operational near real-time fire and smoke detection and characterization program. in W. M. Hao (ed.), *Remote Sensing of Fire: Science and Application*. 2008.

Saide, P. E., D. A. Peterson, A. da Silva, B. Anderson, L. D. Ziemba, G. Diskin, G. Sachse, J. Hair, C. Butler, M. Fenn, J. L. Jimenez, P. Campuzano-Jost, A. E. Perring, J. P. Schwarz, M. Z. Markovic, P. Russell,

Geosci. Model Dev. Discuss., https://doi.org/10.5194/gmd-2017-207
Manuscript under review for journal Geosci. Model Dev.
Discussion started: 6 November 2017

J. Redemann, Y. Shinozuka, D. G. Streets, F. Yan, J. Dibb, R. Yokelson, O. B. Toon, E. Hyer, and G. R. Carmichael. Revealing important nocturnal and day-to-day variations in fire smoke emissions through a multiplatform inversion, *Geophysical Research Letters*, 42: 3609-18. doi:10.1002/2015gl063737, 2015.

Sandberg, D.V., and J. Peterson. A source strength model for prescribed fires in coniferous logging slash, *1984 annual meeting, Air Pollution Control Association, Northwest Section. 14p*. 1984.

Sapkota, A., J. M. Symons, J. Kleissl, L. Wang, M. B. Parlange, J. Ondov, P. N. Breysse, G. B. Diette, P. A. Eggleston, and T. J. Buckley. Impact of the 2002 Canadian forest fires on particulate matter air quality in Baltimore City, *Environmental Science & Technology*, 39: 24-32. doi:10.1021/es035311z, 2005.

Schroeder, W., M. Ruminski, I. Csiszar, L. Giglio, E. Prins, C. Schmidt, and J. Morisette. Validation analyses of an operational fire monitoring product: The Hazard Mapping System, *International Journal of Remote Sensing*, 29: 6059-66. doi:10.1080/01431160802235845, 2008.

Singh, H. B., C. Cai, A. Kaduwela, A. Weinheimer, and A. Wisthaler. Interactions of fire emissions and urban pollution over California: Ozone formation and air quality simulations, *Atmospheric Environment*, 56: 45-51. doi:10.1016/j.atmosenv.2012.03.046, 2012.

Singh, H. B., L. Salas, D. Herlth, R. Kolyer, E. Czech, W. Viezee, Q. Li, D. J. Jacob, D. Blake, G. Sachse, C. N. Harward, H. Fuelberg, C. M. Kiley, Y. Zhao, and Y. Kondo. In situ measurements of HCN and CH3CN over the Pacific Ocean: Sources, sinks, and budgets, *Journal of Geophysical Research-Atmospheres*, 108. doi:10.1029/2002jd003006, 2003.

Sofiev, M., T. Ermakova, and R. Vankevich. Evaluation of the smoke-injection height from wild-land fires using remote-sensing data, *Atmospheric Chemistry and Physics*, 12: 1995-2006. doi:10.5194/acp-12-1995-2012, 2012.

Strand, T. M., N. Larkin, K. J. Craig, S. Raffuse, D. Sullivan, R. Solomon, M. Rorig, N. Wheeler, and D. Pryden. Analyses of BlueSky Gateway PM2.5 predictions during the 2007 southern and 2008 northern California fires, *Journal of Geophysical Research-Atmospheres*, 117. doi:10.1029/2012jd017627, 2012.

Urbanski, S., V. Kovalev, A. Petkov, A. Scalise, C. Wold, and W. M. Hao. Validation of smoke plume rise models using ground-based lidar. in C. M. U. Neale and A. Maltese (eds.), *Remote Sensing for Agriculture, Ecosystems, and Hydrology Xvi*. 2014.

Warneke, C., M. Trainer, J. A. de Gouw, D. D. Parrish, D. W. Fahey, A. R. Ravishankara, A. M. Middlebrook, C. A. Brock, J. M. Roberts, S. S. Brown, J. A. Neuman, B. M. Lerner, D. Lack, D. Law, G. Hubler, I. Pollack, S. Sjostedt, T. B. Ryerson, J. B. Gilman, J. Liao, J. Holloway, J. Peischl, J. B. Nowak, K. C. Aikin, K. E. Min, R. A. Washenfelder, M. G. Graus, M. Richardson, M. Z. Markovic, N. L. Wagner, A. Welti, P. R. Veres, P. Edwards, J. P. Schwarz, T. Gordon, W. P. Dube, S. A. McKeen, J. Brioude, R. Ahmadov, A. Bougiatioti, J. J. Lin, A. Nenes, G. M. Wolfe, T. F. Hanisco, B. H. Lee, F. D. Lopez-Hilfiker, J. A. Thornton, F. N. Keutsch, J. Kaiser, J. Q. Mao, and C. D. Hatch. Instrumentation and measurement strategy for the NOAA SENEX aircraft campaign as part of the Southeast Atmosphere Study 2013, *Atmospheric Measurement Techniques*, 9: 3063-93. doi:10.5194/amt-9-3063-2016, 2016.

Wiedinmyer, C., S. K. Akagi, R. J. Yokelson, L. K. Emmons, J. A. Al-Saadi, J. J. Orlando, and A. J. Soja. The Fire INventory from NCAR (FINN): a high resolution global model to estimate the emissions from open burning, *Geoscientific Model Development*, 4: 625-41. doi:10.5194/gmd-4-625-2011, 2011.

Wiedinmyer, C., B. Quayle, C. Geron, A. Belote, D. McKenzie, X. Y. Zhang, S. O'Neill, and K. K. Wynne. Estimating emissions from fires in North America for air quality modeling, *Atmospheric Environment*, 40: 3419-32. doi:10.1016/j.atmosenv.2006.02.010, 2006.

Wotawa, G., and M. Trainer. The influence of Canadian forest fires on pollutant concentrations in the United States, *Science*, 288: 324-28. doi:10.1126/science.288.5464.324, 2000.

Xu, L., A. M. Middlebrook, J. Liao, J. A. de Gouw, H. Y. Guo, R. J. Weber, A. Nenes, F. D. Lopez-Hilfiker, B. H. Lee, J. A. Thornton, C. A. Brock, J. A. Neuman, J. B. Nowak, I. B. Pollack, A. Welti, M. Graus, C. Warneke, and N. L. Ng. Enhanced formation of isoprene-derived organic aerosol in sulfur-rich power plant plumes during Southeast Nexus, *Journal of Geophysical Research-Atmospheres*, 121: 11137-53. doi:10.1002/2016jd025156, 2016.

Yarwood, G., S. Rao, M. Yocke, and G. Whitten. Updates to the Carbon Bond Chemical Mechanism: CB05, *Technical Report RT-0400675 ENVIRON International Corporation Novato, CA, USA*. 2005.

Zhang, X. Y., S. Kondragunta, and B. Quayle. Estimation of Biomass Burned Areas Using Multiple-Satellite-Observed Active Fires, *Ieee Transactions on Geoscience and Remote Sensing*, 49: 4469-82. doi:10.1109/tgrs.2011.2149535, 2011.